WANDERING THROUGH THE OSTEOCYTE NETWORK OF THE ZEBRAFISH VERTEBRAE: A FIRST ANALYSIS

Faith Maes

Student number: 01803963

Supervisor:	Prof. dr. Paul Eckhard Witten
Counsellors:	Prof. dr. Paul Eckhard Witten, Prof. dr. Ann Huysseune
Research Group:	Evolutionary Developmental Biology, Department of Biology, Ghent University, Ghent 9000, Belgium

Master's dissertation submitted in order to obtain the degree of Master of Science in Biology

Academic year 2024-2025

Word count: 14110 words

GHENT UNIVERSITY FACULTY OF SCIENCES

Wandering through the osteocyte network of the zebrafish vertebrae: a first analysis

Het osteocytennetwerk van de zebraviswervel: een verkennende studie.

Osteocytes, living bone cells inside the bone matrix, are the most abundant bone cells in mammals, regulating bone growth, remodelling, and metabolism through their extensive network. While zebrafish is an established model in biomedical research, most studies on zebrafish bone biology focuses on bone forming cells (osteoblasts) on the bone surface and early developmental stages, prior to the development of osteocytes. This study addresses the knowledge gap of osteocytes in the adult zebrafish skeleton, specifically their morphology, orientation, and distribution within the vertebral column. Using continuous serial parasagittal sections of adult zebrafish. Light microscopy is employed to measure and describe osteocytes and polarized light microscopy to identify the orientation of cell body and cell processes relative to the orientation of bone matrix fibres. Osteocyte processes (or dendrites) form a lacuna-canalicular network. Its strength is assessed by quantifying osteocyte density and evaluating branching of dendritic processes. The study focuses on osteocyte morphology and the distribution of the lacuna-canalicular network between and within regions of the vertebral body. Our data suggest variations in osteocyte size, shape, and distribution within and between vertebral regions. In the vertebral centrum, osteocytes are orientated circumferentially in the outer regions of the biconcave centrum (incl. vertebral body endplates) but parallel to the anterior-posterior body axis in the middle of the centrum, aligning with the orientation of the collagen fibres. In the vertebral body endplates, osteocytes are abundant close to Sharpey's fibres, forming a dense network of dendrites with perpendicular orientation. Neural spine osteocytes have a different morphology. The cells are long and thin with polarized long dendrites parallel to the orientation of the collagen fibres. The study's findings support the initial hypothesis that the type of bone significantly influences the morphology and orientation of osteocytes in zebrafish vertebrae. There is a clear link between osteocyte shape and the orientation of collagen fibres in the surrounding bone matrix. The study also found a strong correlation between areas of high mechanical strain and high osteocyte density, suggesting that osteocytes are mechanosensitive. This study provides first insights into osteocyte morphology, density and organization in vertebral bodies of *Danio rerio.*

Osteocyten, levende botcellen in de botmatrix, zijn de meest voorkomende botcellen bij zoogdieren. Ze reguleren botgroei, herstructurering en metabolisme via hun uitgebreid netwerk. Hoewel de zebravis een courant modelorganisme is in biomedisch onderzoek, richten de meeste studies naar zebravis botbiologie zich op botcellen die bot vormen (osteoblasten), gelegen op het botoppervlak en vroege ontwikkelingsstadia, vóór de ontwikkeling van osteocyten. Deze studie pakt het gebrek aan kennis over osteocyten in het volwassen zebravis skelet aan, specifiek hun morfologie, oriëntatie en distributie binnen de wervelkolom. We maken gebruik van continue seriële parasagittale coupes van volwassen zebravissen om de rugwervels te doorlopen. Lichtmicroscopie is gebruikt om osteocyten te meten en te beschrijven, en gepolariseerde lichtmicroscopie om de oriëntatie van het cellichaam en de cel uitlopers te identificeren ten opzichte van de oriëntatie van de vezels van de botmatrix. Osteocyt processen (of ook wel dendrieten genoemd) vormen een lacuno-canaliculair netwerk. De sterkte hiervan wordt beoordeeld door de osteocyt dichtheid te kwantificeren en de vertakking van dendrieten te evalueren. De studie focust op de osteocyt morfologie en de distributie van het lacuno-canaliculair netwerk tussen en binnen regio's van de wervels. Variaties in osteocyten grootte, vorm en distributie zowel tussen als binnen verschillende wervelregio's werden geobserveerd. De osteocyten hebben een circulaire oriëntatie aan de uitersten van het wervellichaam (de eindplaten), maar zijn parallel met de anteroposteriore as in het midden van het wervellichaam. Dit komt overeen met de oriëntatie van de collageen vezels van de botmatrix. In de eindplaten van de wervelkolom is er een hoge abundantie van osteocyten ter hoogte van de Sharpey vezels met een dens netwerk van dendrieten die daarop loodrecht georiënteerd zijn. Het doornuitsteeksel heeft osteocyten met een verschillende morfologie. Ze zijn lang en dun met gepolariseerde lange dendritische processen die parallel georiënteerd zijn met de collageen vezels. Deze studie presenteert inzichten in osteocyten morfologie, densiteit en organisatie in wervellichamen van *Danio rerio*.

Acknowledgments

I would like to express my deepest gratitude to my supervisor, Professor Eckhard Paul Witten, for his invaluable patience, insightful feedback, and guidance. This journey would not have been possible without him. I am especially grateful for the opportunity to attend the CC&BB conference, where I gained invaluable knowledge about cartilage and bone from some of the most interesting researchers in the field. I also extend my sincere thanks to the reading committee for their time and for providing insightful feedback that will be essential for my future academic endeavours. My thanks also go to Ann Huysseune, who inspired me by her passion for the field, and that spark ignited my own interest in developmental biology. Many thanks to Adelbert De Clercq for his insightful discussions and for guiding me through the talks at my first conference and for his comforting words and support throughout this thesis . Lastly, I would be remiss if I did not mention my close circle of family and friends. To my family -especially my parents, grandparents, and sister- thank you for your unwavering belief in me, which kept me going during challenging times. I am also incredibly grateful for my friends, especially Rik, for always keeping me calm and reminding me to believe in myself.

TABLE OF CONTENT

1 Introduction

1.1 Zebrafish as a model organism

In 1822 Francis Hamilton discovered a "beautiful fish with several blue and silver stripes on each side" in India near the Ganges River (Hamilton, 1822) (Figure 1). Without him knowing, he stumbled on a fish that has become one of the most important laboratory animals to study vertebrate development. Zebrafish (*Danio rerio*) have found their way into the lab because of their transparent embryo's, external fertilization, rapid development, and high fecundity. A fully sequenced genome showed that more than 70 % of zebrafish genes are conserved with humans, and disease-causing genes are with 80%, even more conserved (Kague & Karasik, 2022). Studies by (Moss, 1961) showed similarities in the skeletal morpho-physiology of the zebrafish skeleton with mammalian bone. These so-called "basal" teleosts develop cellular bone in adulthood, meaning their bone contain osteocytes, a feature not found in more advanced teleost's. Today zebrafish is also used as a vertebrate model of choice in biomedical research on bone and bone diseases, such as osteoporosis, at an unprecedented pace (Bek et al 2021; Bonewald, 2010, 2011; Foessl et al., 2021; Kague & Karasik, 2022; Tonelli et al., 2020). As the world population ages, bone diseases are becoming a major medical problem, both economically and in term of public health burden (Kague & Karasik, 2022). The knowledge of gene homology and bone similarity paved the way for the use of Zebrafish in biomedical research and drug testing on bone diseases. However, despite the growing use of zebrafish in bone research, a substantial knowledge gap on the most abundant and long-lived cells -osteocytes- remains. In particular, the abundance, morphology and the spatial organization of the lacuna-canalicular network (LCN) of osteocytes in the zebrafish skeleton remains understudied. Given that the LCN plays a crucial role in bone biology of mammals, this lack of knowledge raises concerns about the translational relevance of zebrafish for bone diseases and the effectiveness of drug treatments (Kague & Karasik, 2022). A more detailed study on the osteocytic network of zebrafish is needed to evaluate the utility as a model organism in skeletal research.

Figure 1: Zebrafish (*Danio rerio*) image by Petr Kuznetsov from Pixabay

1.1.1 Bone function and biology

Among vertebrates, the development of a bony endoskeleton represents a fundamental evolutionary advancement. This characteristic contributed to their diverse range of lifestyles. Bone provides structural support from weight bearing and provides a lever that, in combination with muscle contractions, refines vertebrate movement. Moreover, the skeleton performs functions at the microscopical level, such as reserving essential ions like calcium, phosphates, and magnesium (Burger et al., 1995; Huysseune, 2000). However, different from tetrapods, the endoskeleton of zebrafish and other teleost's is not used as storage for calcium and phosphorus. Calcium can be obtained from the water and phosphorus, in case of need, is mobilised from the dermal skeleton, represented by elasmoid scales (Witten et al., 2017; Witten & Huysseune, 2009).

Bone is composed of two main components: (i) Bone cells, and (ii) a solid extracellular matrix, which itself consists of an organic phase and a mineral phase. The major constituent of the organic phase is type I collagen (Collagen I). Collagen I is a fibrillar protein that provides toughness and viscoelasticity to bone tissue (Totland et al., 2011). Collagen I not only contributes to the structural resilience of bone but also plays a critical role in mineral deposition and the modulation of mechanical strength (Viguet-Carrin et al., 2006). Importantly, the orientation of collagen fibres within the matrix is a major determinant of bone mechanical properties. Initially, bone tissue forms rapidly. This quick deposition leads to randomly oriented Type I collagen fibres, characteristic of what's known as woven bone. As a teleost fish matures, a progressive replacement and formation by more organized bone occurs (Davesne et al., 2020; Witten & Huysseune, 2009). Lamellar or parallel-fibered bone contains collagen fibres aligned according to mechanical loading patterns, with longitudinal fibres in tensile regions and transverse fibres in compressive regions (Davesne et al., 2020; Oxlund et al., 1995; Witten & Huysseune, 2009) (Figure 2).

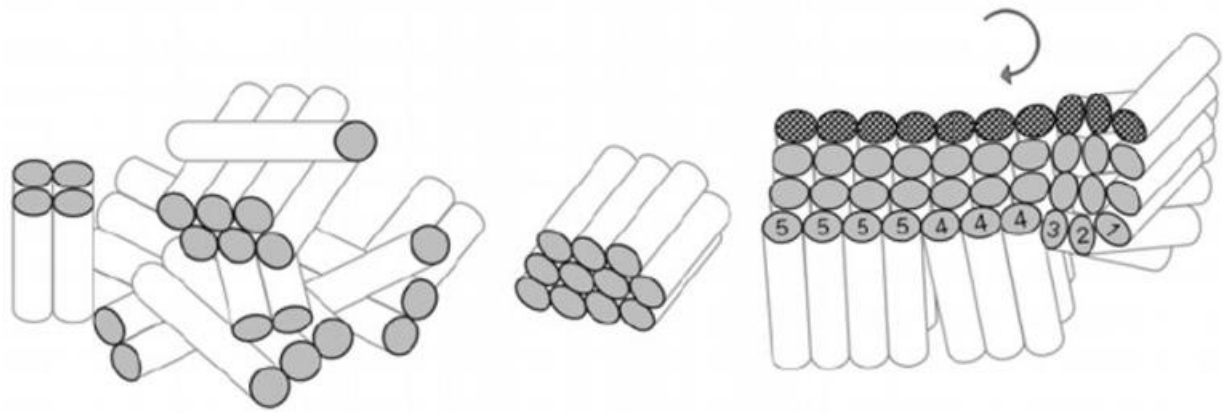

Figure 2. orientation of collagen fibres in bone. (left) woven bone (centre) parallel fibred bone and (right) lamellar bone (Fatima et al., 2011).

Far from being static, the teleost skeleton, like that of other vertebrates, is a dynamic organ of hard tissue that constantly adapts to functional demands (Witten & Hall, 2015). There is ongoing fine-tuning of skeletal elements through bone formation and resorption throughout the vertebrate lifespan. From early developmental stages, where it supports growth, to adulthood and old age, where it maintains the structural integrity of the skeletal elements and regulates mineral homeostasis, bone remodelling remains essential to provide maximal strength with a minimum of bone mass (Burger et al., 1995). As in mammals, teleost bone adapts to use and disuse (Huysseune, 2000; Totland et al., 2011). Bone cells that actively contribute to this bone remodelling work in mammals are collectively referred to as 'basic-multicellular units' or BMUs (Burger et al., 2003). The BMUs consists of two key bone cell types located at the surface of the bone: (i) Osteoblasts, are bone secreting cells derived from precursor cells of mesenchymal origin (Figure 3: MSC) (Bonewald, 2004). They produce osteoid, the precursor of mineralized bone matrix. (ii) Osteoclasts are bone resorbing cells of hematopoietic origin (Figure 3: HSC). In addition two other bone cell types - derived from osteoblasts but not considered BMUs- contribute to bone maintenance: (i) Bone lining cells, differentiated osteoblast that do not produce osteoid, and (ii) osteocytes, the only bone cells within the bone matrix (Huysseune, 2000) (Figure 3). Effective communication among all these bone cell types (via growth factors, cytokines, and hormones) is essential for maintaining the balance between bone resorption and formation and thus ensures a healthy functional bone structure (Bonewald, 2010; Franz-Odendaal et al., 2006).

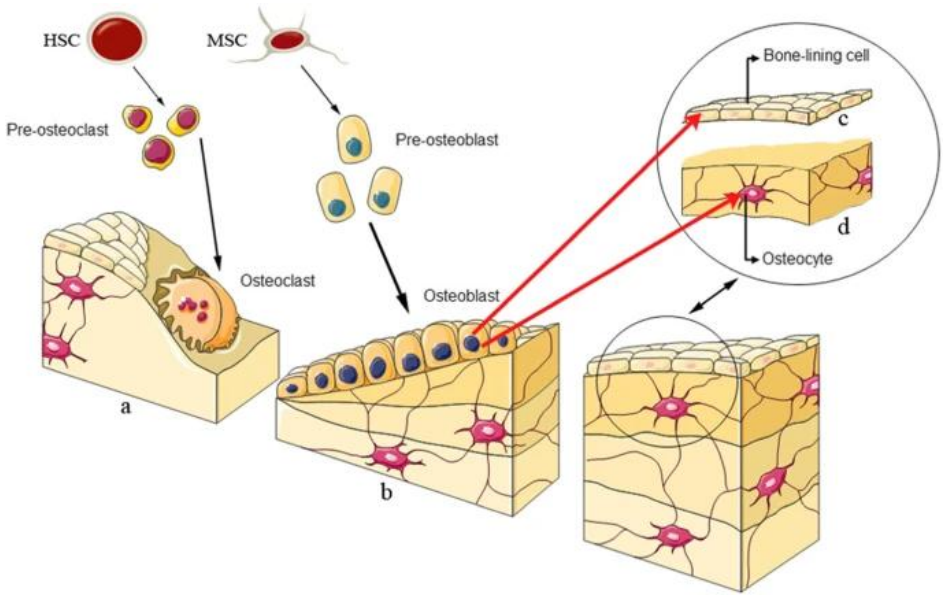

Figure 3. Image portraying different type of bone cells. a: osteoclasts originate from hematopoietic stem cell, these cells destruct weary and ancient bone,. B:. osteoblasts originate from mesenchymal stem cell that differentiates to the bone-lining cell and osteocyte. C: bone lining cell D: osteocyte. (Amirazad et al., 2022)

1.2 Osteocytes

Osteocytes are defined by their location within the bone matrix. Differentiation into osteocytes, which are osteoblast descendants, occurs via osteocytogenesis (Bonewald, 2011). During this process, osteoblasts become encapsulated by newly formed osteoid, eventually maturing into osteocytes (Figure 4). How osteoblasts get buried in the bone matrix, is not yet fully understood. However, it seems to depend on the mode of ossification and differs between bone types (Franz-Odendaal et al., 2006). After encapsulation, further differentiation from osteoblast to osteocytes leaves cavities in the bone matrix called lacunae wherein the cell body resides. Numerous dendritic processes extend from this cell body into thin channels throughout the bone matrix called canaliculi (Franz-Odendaal et al., 2006). Lacunae and canaliculi form an extensive connective network throughout the mammalian bone, comparable in length to that of the nerve fibres in the human brain (Buenzli & Sims, 2015). The increased focus on osteocytes in research was long overdue, given that they are the most abundant cells in mammalian bone. Recent studies showed the role of osteocytes as a director for osteoclastic resorption, both in healthy bone and under pathological conditions, leading to the increased demand for studies regarding their role in bone diseases like osteoporosis (Bonewald, 2004; Bonucci, 2009; Burger et al., 2003; Kague & Karasik, 2022).

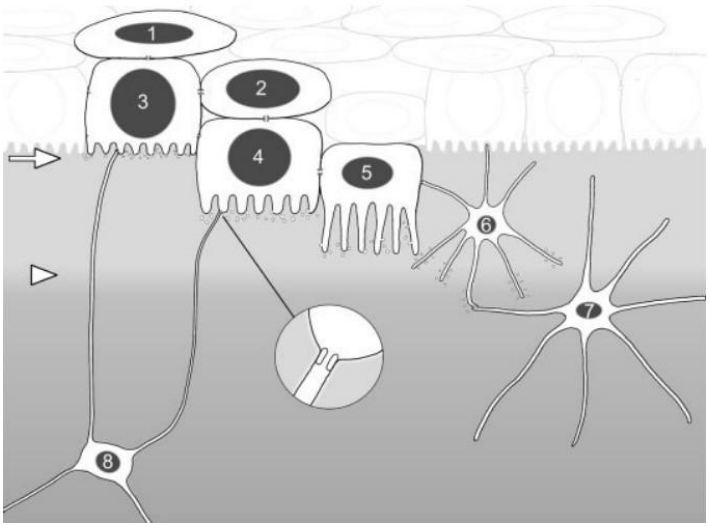

Figure 4. Diagram showing the transitional cell types between preosteoblasts and osteocytes during osteoblast transformation. The diagram is not to scale. 1. Preosteoblast, 2. Preosteoblastic osteoblast, 3. Osteoblast, 4. Osteoblastic osteocyte (type i) (Franz-Odendaal et al., 2006)

1.2.1 Osteocyte functions

Osteocytes are the key functional cells for remodelling of the mammalian skeleton. According to Haridy et al. (2021) Osteocytes have two functions: (i) Mechanical homeostasis as well as (ii) mineral homeostasis of the skeleton.

Due to their morphological traits, osteocytes are key drivers in mechanical homeostasis, of the bone. They are the major mechano-sensing cells of bone, detecting strain (i.e. deformation by the stretching or compression) in the bone matrix as well as fluid shear stress (i.e. the frictional force exerted by fluid moving across their surface) within the lacunar-canalicular network, both of which result from mechanical loading (Knothe Tate et al., 2004). This mechano-sensing is caused by two main mechanisms as a clear result of their morphology and surroundings. First, Osteocytes are surrounded by a pericellular matrix (Creecy et al., 2021). It is a thin gel-like extracellular matrix layer surrounding the osteocytes, consisting of various molecules, including proteoglycans and collagen VI (Pei et al., 2021). It acts like a medium, transmitting fluid shear stress to the osteocyte cell membrane and regulates molecular transport (Wang, 2018). Secondly, tethering filaments connect dendrites with the canalicular wall. Hereby amplifying shear drag forces by fluid flow and causes mechanical stimulation of osteocytes. Alongside detecting mechanical cues in the lacuna-canalicular network, osteocytes communicate with one another and osteogenic cells on the surface to guide bone remodelling (Burger et al., 1995, 2003). Mechanotransduction is defined as the translation of detected mechanical forces into biochemical signals, including the subsequent solute transport of these signalling molecules through the LCN via hemichannels and gap junctions (Bonewald, 2010, 2011; Bonewald & Johnson, 2008) (Figure 6).

In addition, osteocytes participate in mineral homeostasis, particularly in tetrapods. The skeleton is an important reservoir of minerals such as calcium, phosphates, and magnesium, which are needed in the blood for normal functioning of the body. Osteocytic osteolysis is a reversible, localised process of matrix removal by osteocytes around their lacuna, causing a continuous change of their lacuna shape. Osteocytes control the local and direct calcium levels in mammalian bone, whereas osteoclasts can access calcium on a longer time scale. Although this mechanism was proposed already over one hundred years ago, there is still a lot of criticism on the topic (Shahar & Dean, 2013). The lacunar enlargement in mammals during lactation is pronounced in bats *(Myotis lucifuguf)* and in other calcium deprived states (Kwiecinski et al., 1987). The study on bats clearly supports the hypothesis and the involvement of osteocytes in calcium homeostasis in mammalian bone (Bonewald, 2011; Qing et al., 2012). However, methods to evaluate size of lacunae can incorrectly indicate enlargement of osteocytes and their integrity and functional relevance in teleost's remains uncertain (Bonucci, 2009).

Most teleost species have acellular bone (i.e. bone entirely devoid of osteocytes) (Davesne et al., 2019; A. M. de Azevedo et al., 2025; T. P. de Azevedo et al., 2012) (Figure 5). The skeleton of most, but not all, teleost species is composed entirely of either cellular or acellular bone, and closely related species mostly share the same bone type (Moss, 1961). In teleost species with cellular bone, such as zebrafish, early stages are acellular. Huysseune (2000) hypothesized that osteocyte distribution and morphology depend on the bone matrix volume, explaining the absence of osteocytes in thin cranial bones and small skeletal elements of young individuals. In the zebrafish skeleton osteocytes appear in the bone matrix at about 30 days post fertilisation and their appearance coincides with the start of bone remodelling (Witten et al., 2001). Apart from the absence of osteocytes, acellular bone and cellular bone are remarkably similar. Both undergo active remodelling by BMUs; however, osteoclasts are structurally different in both bone types (Witten & Huysseune, 2009). The ability of acellular bone to undergo remodelling raises questions about the extent to which zebrafish osteocytes engage in mechano-sensing and signalling.

Evolution to acellular bones within the teleost clade could be explained by their aquatic lifestyle. Aquatic animals can mobilise calcium and other elements directly from their surrounding waters. Further, it has been suggested that osteocytes in advanced teleost got lost during a long marine evolutionary history. Primary freshwater fish such as zebrafish have osteocytes whereas secondary freshwater fish, decedents from marine ancestors such as cichlids, have lost osteocytes (Witten & Huysseune, 2009). A deeper characterization of osteocytes and their distribution in bone in *Danio rerio* could help understand the evolutionary acellularization process within the Teleostei.

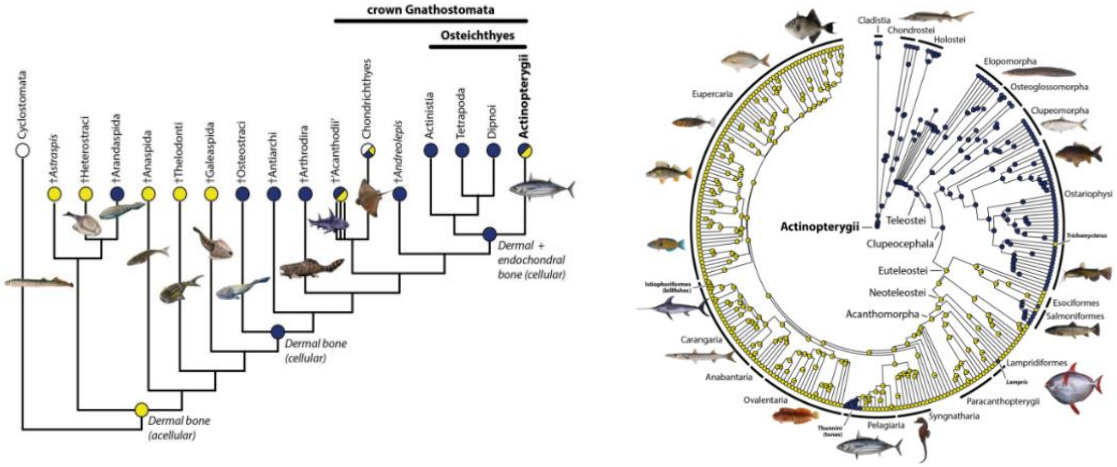

Figure 5. Distribution of cellular and acellular bone in the phylogeny of vertebrates (modified from Keating et al., 2018). the coloured circles at the tip of branches reflect bone type in the clade: acellular (yellow), cellular (dark blue), or bone absent (white) (Davesne et al., 2019).

1.2.2 Osteocyte Morphology

Research has identified two osteocyte types associated with morphology, with some assuming distinct functions inside teleost cellular bone (Weigele & Franz-Odendaal, 2016). They are referred to as Type I and Type II osteocytes. Both osteocyte types seem to coexist within the skeleton with variation at different scales (i.e. within single bone, among bones within an individual, among individuals of different developmental life stages, among species) (Bonucci, 2009; Davesne et al., 2020; Weigele & Franz-Odendaal, 2016).

Type I osteocytes have round or irregular-shaped cell bodies with omnidirectionally or radially protruding dendritic processes branching in canaliculi (Kerschnitzki et al., 2011). They are mostly referred to as star-shaped osteocytes in literature. Davesne et al. (2020a) studied the 3D characterization of osteocytes at different scales in Actinopterygii. They proposed that putative woven bone is characterized by great variability in shape, orientation, and distribution of this osteocyte type. Within this bone type there is almost no mutual alignment between osteocytes and no long-range order of the ECM orientation.

Secondly, Type II osteocytes have a spindle-shaped/elongated cell body following the orientation of the collagen fibres in the ECM of mammalian bone (Davesne et al., 2020; Kerschnitzki et al., 2011) (Figure 6). Davesne et al. (2020a) proposed that this Type II morphology in combination with an even distribution and orientation of the osteocytes corresponds with organized bone (i.e. parallel-fibred or lamellar bone). As such they are located closer to the outer bone surfaces. Cytoplasmic processes are oriented into two orders, the first orientated aligning with the long axis and the second perpendicular on the long axis and the ECM orientation. Totland et al. (2011) question the strength of the canalicular system for Type II osteocytes in Salmon.

Studies suggested differences in cell volumes for different bone types. The volume of osteocyte lacunae in woven bone were found to be larger than in putative organized bone within a skeletal element in Actinopterygii. Variation between within the same bone typology is hypothesized to be caused by variation in growth rates throughout time (Davesne et al., 2020). However, only a handful of studies have focused on the morphology of osteocytes in zebrafish bone. Given their intriguing position in evolution and their value in biomedical research, there is a strong need for attention to osteocytes in this model organism.

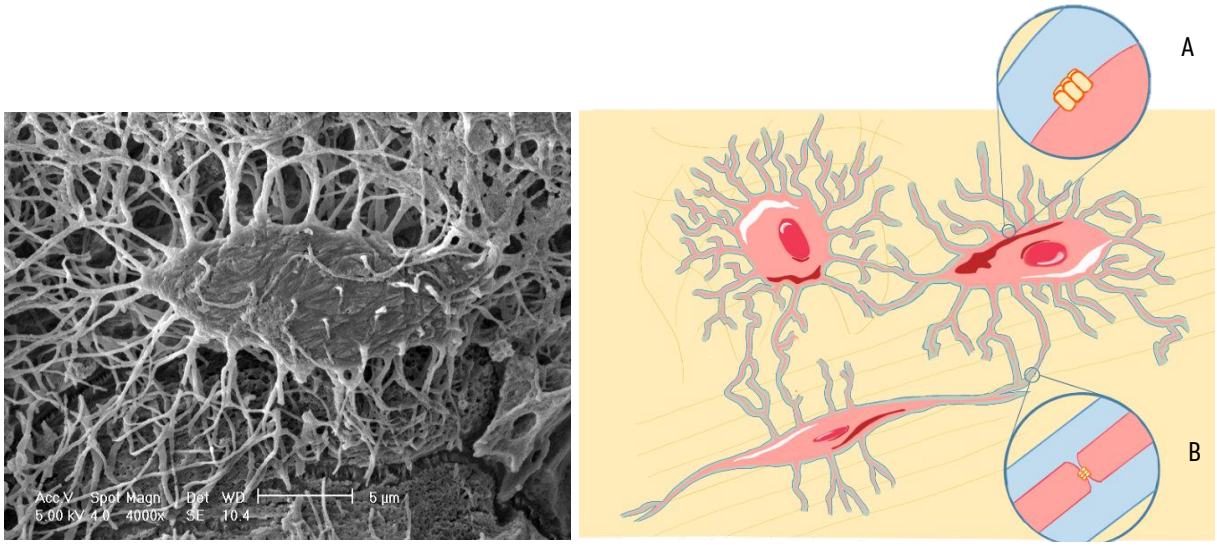

Figure 6: (Left) A close-up of an osteocyte within the bone (Mus Musculus) © Bonewald, Lynda. (Right) Schematic drawing of osteocyte varying shapes in the bone matrix. Dark yellow lines represent collagen fibre orientation (not to scale). A: Hemichannel, B: Gap junction (drawing created in Procreate).

1.3 Vertebra

The vertebral column, composed of vertebrae and intervertebral disks, serves as an advantageous model for investigating osteocyte biology in zebrafish. Zebrafish vertebrae are specifically adapted to withstand the mechanical strains generated during swimming (Totland et al., 2011). This inherent mechanical loading makes them a relevant system for studying osteocytes also shown in swim training experiments of rainbow trout by Deschamps et al. (2009). They demonstrated that vertebral bone tissue, including mineral content and remodelling processes, is affected by use and disuse of bone (Suniaga et al., 2018).

The zebrafish vertebra, like that of other Teleostei, is composed of a vertebral body (vertebral centrum) and associated extensions. The morphology of these structures varies among species and along the vertebral column.

The vertebra is primarily formed by two ossification centres. The autocentrum forms the internal, hourglass-shaped structure, the vertebral centrum (C), observed across teleost species, as well as a lateral plate at each side of the vertebra (LT) (Figure 7) (Peskin et al., 2020). This central component provides axial strength and articulation between vertebrae. The external morphology of the arcocentrum exhibits great interspecies variation (Martini et al., 2023; Sakashita et al.,

2019). In zebrafish, the arcocentrum is composed of ventral and dorsal extensions, which include the neural (NA) and haemal arch (HA) and spine (NS and HS) (Figure 7). It also includes plate-like trabeculations, specifically the left and right ventro- and dorsolateral plates (DT and VT) (Figure 7) (Martini et al., 2023).

The neural arch (NA) encloses the spinal cord, extending dorsally into the neural spine (NS) and attached to the dorsal rim of the endplate. In the caudal region, the haemal arch encloses the caudal artery and vein, extending ventrally into the haemal spine. These arches and their associated spines provide sites for muscle attachment, facilitating swimming movement (Bird & Mabee, 2003; Martini et al., 2023). The vertebral arches form separately from the vertebral bodies through intramembranous ossification of mesenchymal cells also derived from the sclerotome, later they fuse with the vertebral body (Peskin et al., 2020).

Articular processes known as zygapophyses contribute to the stability and controlled movement of the vertebral column. These include the anterior prezygapophyses (D-pr and V-pr) and posterior postzygapophyses (D-po and V-po), which interlock with adjacent vertebrae on both the neural and haemal arches in the caudal region (Figure 7) (Martini et al., 2023).

This research will specifically focus on the vertebrae of the caudal region in zebrafish. These vertebrae are characterized by (i) Well-developed neural arches with neural spines and haemal arches with haemal spines. (ii) Trabeculation on the dorsal, ventral, and lateral regions of the centrum (Martini et al., 2023). These trabecular networks within the vertebral body are thought to contribute to resisting compressive and shear forces, making them an interesting site to study osteocyte distribution and morphology. Kague & Karasik (2022) highlighted the importance of exploring trabecular bone in zebrafish for biomedical research, as zebrafish lack long bones, which are important sites for bone disease phenotypes in humans. However, trabecular plates have no typical spongious network in the *Danio rerio* vertebrae (Martini et al., 2023).

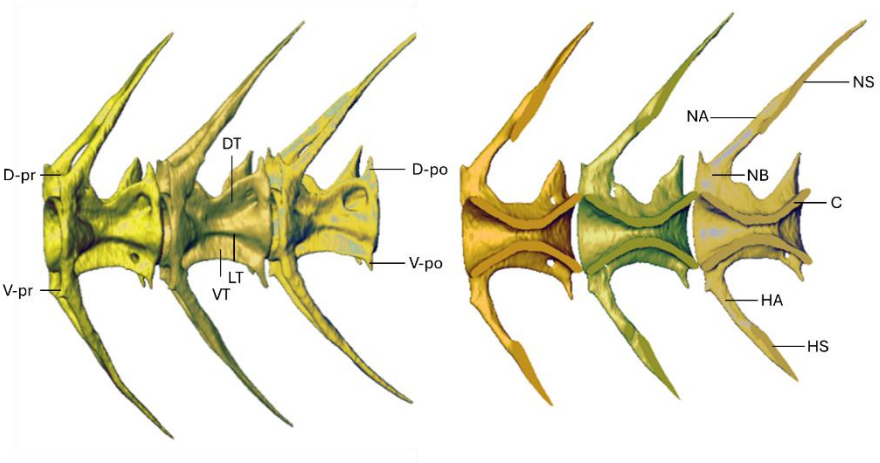

Figure 7. Morphology of caudal vertebrae in zebrafish. (Left) A 3D rendered image of three caudal vertebrae, showing the overall structure. (Right) A parasagittal midline section of the same three caudal vertebrae, revealing internal anatomical details. Abbreviations: D-pr: dorsal prezygapophyses, D-po: dorsal postzygapophyses, V-pr: ventral prezygapophyses, V-po: ventral postzygapophyses, DT: dorsal trabeculation, VT: ventral trabeculation, LT: lateral trabeculation, NS: neural spine, NA: neural arch, NB: neural base, HA: haemal arch, HS: haemal spine, C: centrum. (Scale bar for reference: 100 µm)

2 Objectives

This study focusses on the distribution of and the morphological features of osteocytes in the vertebrae of zebrafish. The primary objectives are:

1. To perform a detailed morphological characterization of osteocytes across distinct regions of the zebrafish vertebrae.
2. Asses the structural integrity of the lacuna-canalicular network (LCN) in the zebrafish vertebrae.

To achieve these objectives, the following sub-objectives are pursued:

1. Identify distinct osteocyte morphotypes based on their spatial distribution in the vertebrae.
2. Investigate the relationship between osteocyte morphology, and collagen fibre arrangement.
3. Quantify osteocyte density and assess its regional variation within the vertebrae.
4. Characterize the dendritic branching patterns of osteocytes and densities.

Based on current literature and preliminary observations, the following hypotheses are falsified:

Bone typology will significantly influence osteocyte shape and the orientation of both the cell body and dendritic processes. Specifically, we expect that osteocytes will closely follow the orientation of collagen fibres in organized bone, while displaying less pronounced alignment in woven bone (Davesne et al., 2020a; Kerschnitzki et al., 2011).

Osteocyte volume and shape will vary between bone types and distinct vertebral regions, correlating with differences in bone matrix volume and mechanical loading (Huysseune, 2000).

Regional variation in osteocyte density will be observed within the vertebrae, dependent on local bone matrix volume and mechanical loading.

Reports about a low degree of dendritic branching and connectivity and a poorly developed LCN in zebrafish (Cao et al., 2011) are falsified.

Table 1: Schematic representation of objectives.

Objectives		
1. Morphological characterization across and within distinct regions 2. Asses the structural integrity of the LCN		
Study focus	**Hypothesized drivers**	
Bone typology	Collagen fibre arrangement	Speed of depositioning
Regional variation	Bone matrix volume	Mechanical load differences
Parameters observed		
Shape	Dendritic complexity	Volume	Density	Orientation

3 Material and Methods

Given the limited existing knowledge on zebrafish osteocyte morphology and distribution across regions of the vertebral column, an initial quantitative data analyses was performed to investigate regional differences. A qualitative observational study was deemed appropriate for comprehensive characterization of osteocytes. The findings on osteocyte morphology and orientation are described for each region sequentially, in alignment with the parasagittal sections, to comprehensively illustrate the 2D microscopic features.

3.1 Histology

In this study, high resolution histology is used to visualize osteocytes and their dendritic processes within zebrafish bone (Foessl et al., 2021). This technique provides both qualitative and quantitative information regarding the osteocyte context within the extracellular matrix. Specifically, it allows for the observation of osteocytes, their dendritic processes, and the branching of these dendrites throughout the entire vertebra. Furthermore, histology enables the acquisition of information about the extracellular matrix, including the possibility of distinguishing between mineralized and non-mineralized bone through specific staining techniques. This capability is crucial for future studies utilizing reporter lines. By means of polarized light microscopy it is possible to obtain information on the orientation of the collagen fibres in the extracellular matrix and bone typology (Foessl et al., 2021).

3.2 Specimen

We obtained already prepared parasagittal sections of a zebrafish body from the Evolutionary Developmental Biology department of Ghent University (Evolutionary Developmental Biology, Department of Biology, Ghent University, Ghent 9000, Belgium) where the research was conducted.

The study was performed on an adult female zebrafish. The specimen was decalcified and embedded in glycol methacrylate (GMA). Prior to sectioning, the head and body (including the abdominal and caudal regions) were separated. Parasagittal sections were cut at a thickness of two micrometre. For each region, four consecutive sections were mounted per glass slide. Every two slides (i.e. four consecutive sections) were stained with Toluidine Blue, leaving a gap of four unstained sections between stained series. Reconstruction of osteocytes are based on four consecutive stained sections.

3.3 Data acquisition

3.3.1 Microscopy

All images were collected on a ZEISS Axio Imager.Z1 equipped with a ZEISS Axiocam 503 color camera. Images acquisition and control were performed using ZEN2 (ZEISS) software. An overview image was made for each vertebrae using a 2.5X objective lens under transmitted light. Detailed images were made under higher magnification of different regions of the vertebrae with a 40X lens to do a quantitative and qualitative analyses of the osteocytes and a 63x/1.4na oil immersion DIC lens was used to observe dendritic processes if needed. Polarized light microscopy was employed to assess the orientation of collagen fibres in the bone matrix.

We followed three caudal vertebrae throughout the specimen. Images were made of stained consecutive slides of these three vertebrae until reaching the midpoint. We considered to be in a midsagittal section of the vertebrae when observing a notochordal outpouching and capturing the fully visible vertebral canal within the hourglass- shaped vertebral centrum. Studying only half of each vertebra was deemed sufficient due symmetry of the vertebrae and owing to the time constrains

of the one-year master's thesis project and the exploratory nature of this pilot study on the histological characterization of osteocytes in zebrafish.

3.3.2 Labelling and measurements

703 osteocytes were labelled according to the regions in the vertebra in which they were identified. The following parameters were considered during this labelling process: (i) Region, the specific anatomical area within the vertebrae where the osteocytes were located. (ii) Characterization of sectioning of the osteocytes, whether they are fully sectioned or incompletely sectioned as well as the orientation of the sectioning (i.e. longitudinal or transverse).

In cases where the same osteocyte was observed across consecutive slides, it was assigned the same label as initially identified. However, after a gap of four slides, osteocytes observed in the same location were treated as 'new' osteocytes, provided they were not sectioned transversely.

3.3.2.1 Defined regions

In this study we define vertebral regions as followed. The vertebral centrum encompasses the end plates and the hour-glass shaped vertebral body centrum. The neural base encompasses all bony structures that connect the neural arch with the vertebral centrum including the pre-neural zygapophyses. The neural base and dorsal trabeculation are distinguishable due to there perpendicular fibre orientation at transition site. The neural arch Is the 45-degree protruding dorsal extension of the vertebrae, we make a distinction between the neural arch and the neural base when the spinal canal is visual. The neural arch and neural spine are distinguishable within the fusion region on histological slides due to slight coloration differences caused by the Toluidine Blue staining. The dorsal trabeculation comprises the post-neural zygapophyses and the trabecular dorsal plate. Transition between neural base and dorsal trabeculation is identifiable by change in collagen fibre orientation from vertical or shifted to 45-degree orientation to horizontal orientation. Similarly, the ventral trabeculation includes the post-haemal zygapophyses and the trabecular ventral plate, with the transition from the haemal arch to the ventral trabeculation identifiable through change in collagen fibre orientation. The lateral trabeculation demonstrates a clearly observable transition from the endplate to the trabecular region due to perpendicular collagen fibre orientation. All studied regions are shown in Figure 9, in both a 3D colour scheme and on histological sections for clarification.

3.3.2.2 Measurement

For the measurement and analysis of each osteocyte, we assessed the long axis and small axis of 703 osteocyte in one single vertebra hemi section. For osteocytes present across multiple consecutive sections, the long and short axes were measured on each relevant slide, resulting in a total of 2940 manual measurements of osteocyte sections. Each osteocyte section was categorized as either completely sectioned (longitudinal or transverse) or incompletely sectioned. Largest measurements of the small and long axis of completely sections were used in analyses as these resemble the highest approximation of the diameter and length respectively (example: Figure 8). These measures were used in analyses to obtain insights on different morphotype osteocytes in regions of the vertebrae. Length/diameter ratios were analysed to get an impression of the 3-dimensional shape of the osteocytes. A ratio closer to zero indicates a more spherical shape. Higher ratios indicate greater lengths and/or lower diameters characterized by a spindle shaped elongated morphology. Assuming osteocytes have an ellipsoid shape, we calculated their volume using the formula $V = \frac{3}{4} * \pi * a * b * c$. Here, a represents the long axis, while b and c represent the short axes. We assumed b=c, effectively treating the osteocyte as an oblate spheroid for volume calculation, where a transverse section perpendicular to the long axis would appear circular. This offers a representative measure of the osteocyte's spatial volume.

Additionally, for each region of the vertebrae, the total area of all stained sections was measured. These area measurements were used to estimate the area density of each bone region. Cellularity (density of the osteocytes) in each

region was obtained by dividing the obtained area with the osteocytes count in the region, allowing for a comprehensive assessment of the spatial distribution and density of osteocytes within the vertebra.

All measurement were done using FIJI software (Schindelin et al., 2012). Calculation of the length of the long and short axis of each osteocyte was done using the straight-line function of the software. Regional area was quantified using the polygonal selection function in FIJI. Some osteocytes were irregularly shaped, therefor long, and short axis were determined subjectively by the researcher via visual evaluation. To minimize the error and increase consistency in lengths and areas, only one researcher took measurements.

3.4 Analyses

All data analyses and plots were performed in R (RStudio) (e.g. “R version 4.2.1, Rstudio 2024.09.01”). We compared the length, width, and volume of osteocytes in each region of the vertebrae. Prior to conducting statistical tests, assumptions of normality, independence, and homogeneity of variances were assessed. Normality was evaluated with the Shapiro-Wilk normality test. Homogeneity of variances was assessed using Levene's test. Based on assumption testing, we performed different statistical approaches to compare osteocytes morphology across different regions of the vertebrae:

(i) If assumptions of normality and homogeneity of variances were met, a one-way Analysis of Variance (ANOVA) was performed. Post-hoc comparisons were conducted using Bonferroni's correction to adjust for multiple comparisons. (ii) If the assumption of homogeneity of variances was violated but normality was met, Welch's ANOVA was used, followed by Games-Howell post-hoc tests for pairwise comparisons. (iii) If assumptions of normality were violated, or if both normality and homogeneity of variances were violated, the Kruskal-Wallis H test was performed. Significant Kruskal-Wallis results were followed by Dunn's test for pairwise multiple comparisons, with p-values adjusted for multiple comparisons.

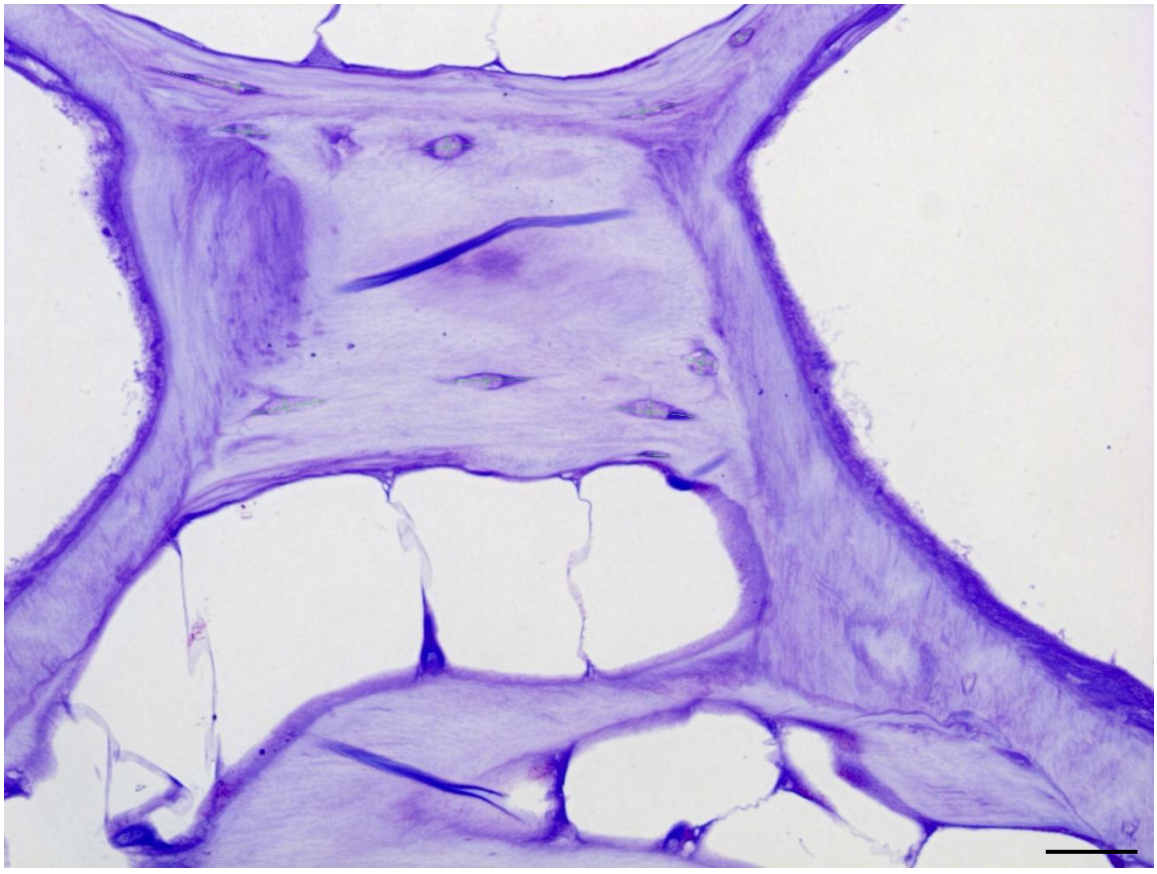

Figure 8. Example of measured osteocytes in the central part of the vertebral centrum with green lines the length and width of the sectioned osteocytes (Scale bar: 20 µm).

a)

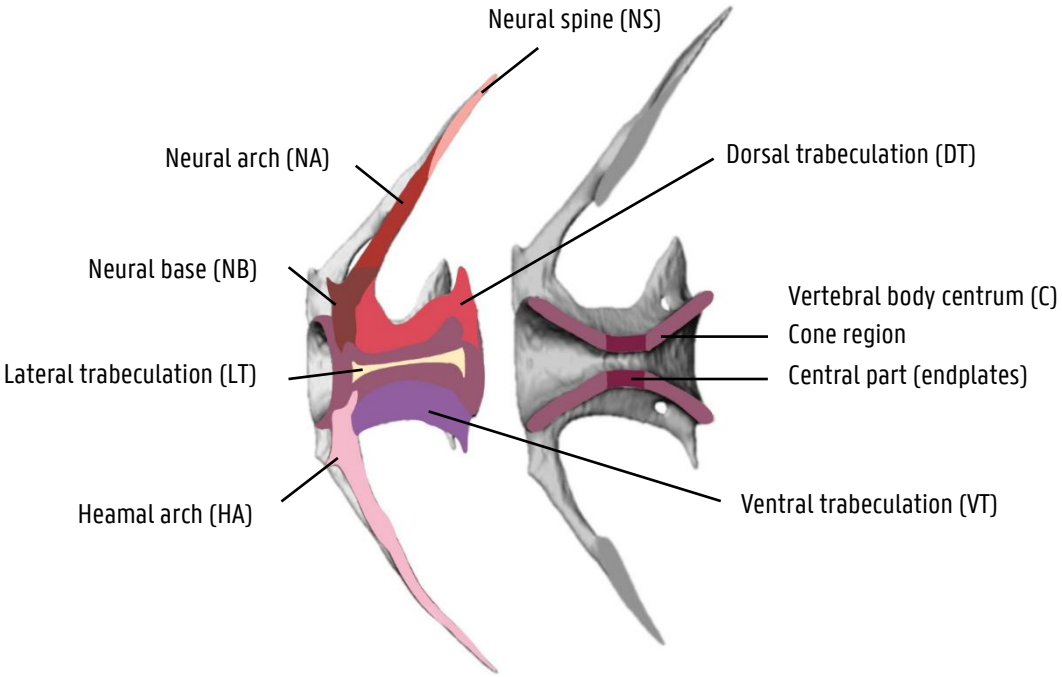
Neural spine (NS)
Neural arch (NA)
Dorsal trabeculation (DT)
Neural base (NB)
Vertebral body centrum (C)
Cone region
Lateral trabeculation (LT)
Central part (endplates)
Heamal arch (HA)
Ventral trabeculation (VT)

b)

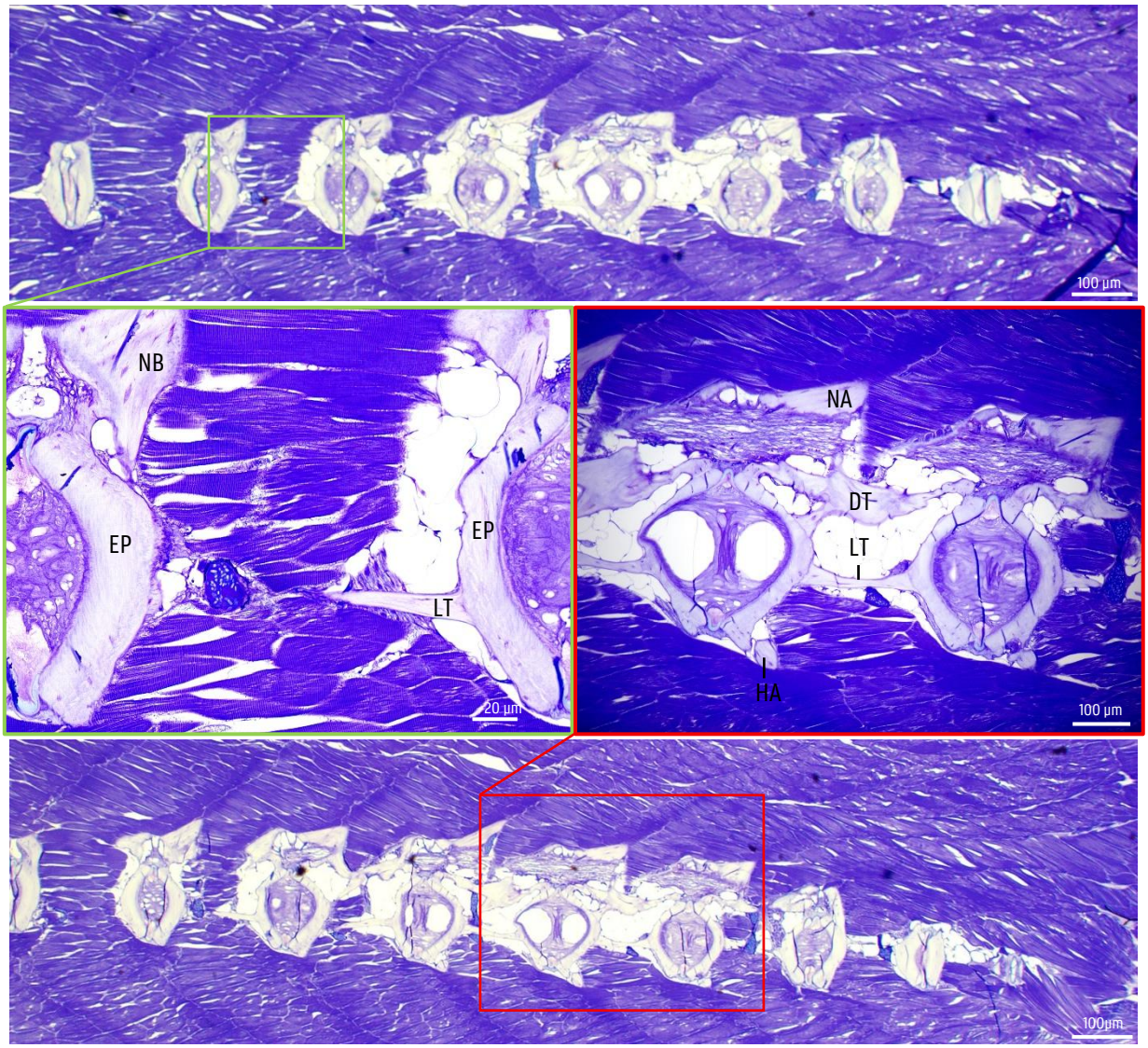
100 µm
NB
EP
EP
LT
20 µm
NA
DT
LT
HA
100 µm
100µm

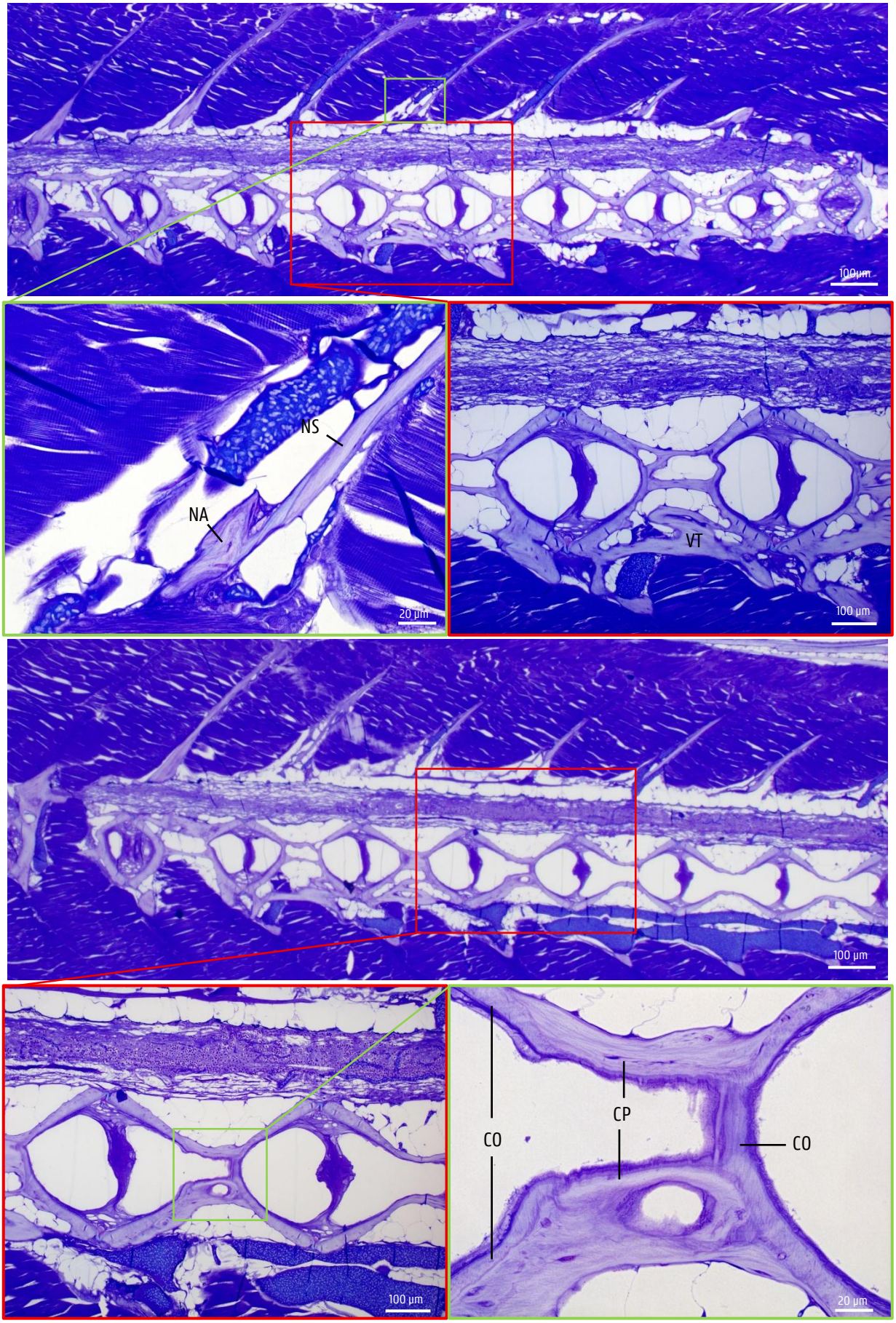

Figure 9. (a) 3D scheme of defines regions that are studied in this paper. (b) histological section of the vertebrae body with each time an overview picture of the spine of the zebrafish and a close-up of the vertebrae. All regions are indicated with abbreviations. Close ups are indicated with boxes on the overview picture. Abbreviations: D-pr: dorsal prezygapophyses, D-po: dorsal postzygapophyses, V-pr: ventral prezygapophyses, V-po: ventral postzygapophyses, DT: dorsal trabeculation, VT: ventral trabeculation, LT: lateral trabeculation, NS: neural spine, NA: neural arch, NB: neural base, HA: haemal arch, C: centrum, EP: endplates, CP: central part of centrum, CO: Cone of centrum.

4 Results

4.1 Qualitative analyses

4.1.1 Centrum: consisting of endplates and biconcave vertebral body

In the lateral part of the endplates, we observe longitudinal sections of long, spindle-shaped osteocytes (Figure 10a/b). The dendritic processes of these osteocytes project perpendicularly from the cell body as well as extend from the osteocyte poles. Dendrites extending from the poles follow the orientation of the cell body axis. Dendritic branching patterns vary, occurring anywhere from the proximal regions near the base of the primary dendrite to its more distal extremities. We only observed dichotomous branching events of these osteocytes (Figure 10b). Secondary dendrites demonstrate an orientation parallel to the primary dendrites from which they arise.

Dendritic processes radiating perpendicularly from the osteocyte cell body tend have a short, thick dendritic base (Figure 10b). Dendritic arborization presented as either dichotomous or trichotomous (Figure 10b) branching events. Secondary dendrites are oriented perpendicularly to the primary dendrites and align with the long axis of the osteocytes. I also observed a high density of "free" dendritic processes, that could not be traced back to the originating cell, oriented perpendicularly to Sharpey fibres in slides showing the lateral sectioning of the endplate (Figure 10a).

As I continued the analysis, advancing through the parasagittal sections toward the midline, osteocytes at the dorsal and ventral sides were incompletely sectioned or had an oval outline. In these sections, fewer dendritic processes were observed radiating from the cell body. However, those incomplete osteocyte sections that included visible poles still showed dendritic processes radiating from those poles.

In the midline sections, osteocytes exhibited a small, round morphology, indicative of a transverse sectioning plane These osteocytes were found clustered at the dorsal and ventral endplate margins, irregularly distributed throughout the bone matrix in close proximity to the Sharpey fibres (Figure 10c). The observed persistence of these cells across more than twelve consecutive 2µm-thick sections suggests a substantial longitudinal dimension exceeding 24 µm. This finding is consistent with the length measurements of elongated osteocytes observed in the lateral parasagittal sections of the endplates (4.2.1.1). Furthermore, osteocyte density was uniform across the anterior and posterior endplates.

Osteocytes within the biconcave vertebral body centrum exhibit distinct orientational patterns. In the central region, osteocytes are predominantly aligned with the longitudinal axis of the vertebrae (Figure 10c). This orientation differs from that of osteocytes at the anterior and posterior vertebral margins, which display a circumferential alignment (Figure 10c). Notably, this pattern of osteocyte orientation is consistent with the change in collagen fibre orientation observed throughout the vertebral body, as evidenced by polarized light microscopy (Figure 11).

In the central region of the vertebral body, osteocytes are typically spindle-shaped (Figure 10d). Dendritic processes radiate perpendicularly from the cell body's long axis, and secondary dendrites are oriented horizontally, mirroring the surrounding fibre orientation. Pole-extending dendrites also occur in these osteocytes. Additionally, osteocytes with a more irregular, or rounder shape are occasionally observed (Figure 10d). These are primarily found in transitional zones where fibre orientation shifts (Figure 11), as well as in the fusion regions of the centrum and trabeculations (Figure 10c). These rounder osteocytes, dendritic branching appears less organized, and dendritic processes tend to be longer.

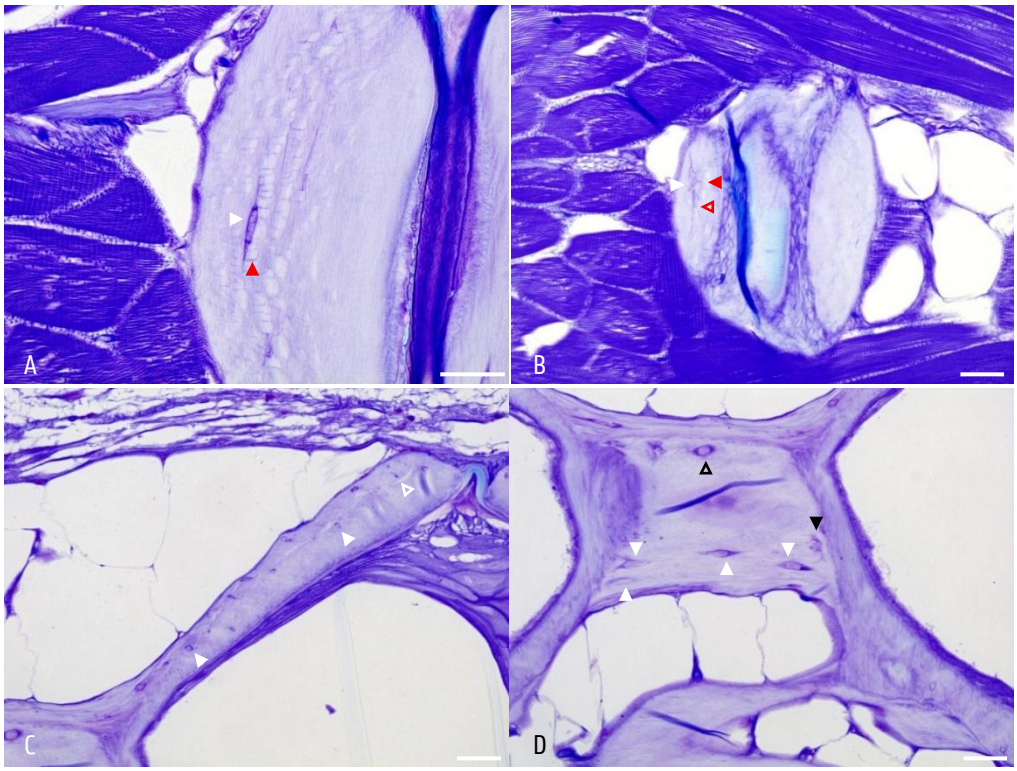

Figure 10: Light microscopy images of osteocytes in various regions of the vertebral centrum. (A) Spindle-shaped osteocyte (solid white arrow) located in the anterior endplate. Note the dendritic processes (solid red arrow) emanating from the cell body and extending perpendicular to the Sharpey fibres. (B) Another spindle-shaped osteocyte (solid white arrow) in the anterior endplate. The dendritic processes show both dichotomous branching (hollow red arrow) and perpendicular extensions from the cell body. A primary perpendicular dendrite displays trichotomous branching (solid red arrow), with secondary dendrites aligned parallel to the osteocyte's long axis. (C) Transversely sectioned osteocytes (solid white arrows) in the dorsal part of the posterior cone. These cells are in close proximity to the Sharpey fibres (hollow white arrow). (D) A mix of spindle-shaped (solid white arrow) and round osteocytes (solid and hollow black arrows) in the central region of the vertebral centrum. A round osteocyte (solid black arrow) is located in a transitional region of abruptly shifting fibre orientation. Another round osteocyte (hollow black arrow) is found where the centrum and dorsal trabeculations fuse, a region with a similar fibre orientation (All scale bars: 20 µm).

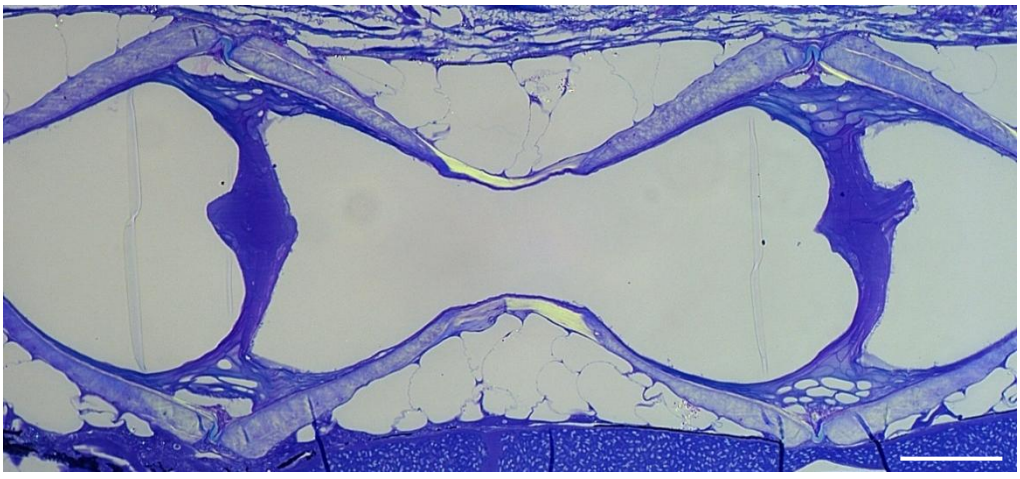

Figure 11: Polarized light microscopy of a parasagittal midline section of a vertebral body. This image illustrates the distinct change in collagen fibre orientation between the outer cone regions and the central region of the vertebral body (scale bar: 100 µm).

4.1.2 Dorsal outgrowth

4.1.2.1 Neural base

The neural base extends upwards on the lateral side of the endplates (Figure 12a). In this transitional region, osteocytes are orientated upward, following the orientation of the collagen fibres. They are spindle-shaped, with dendritic processes

extending from their poles as well as perpendicular on the cell body. From these primary dendrites, secondary dendrites emerge perpendicularly before turning to align with the long axis of the osteocyte. Dendritic arborization occurs through either dichotomous or trichotomous branching.

Osteocytes homogeneously arranged across the neural base, extending from near the bone surface up to deep within the bone matrix. Proximally along the neural base, where a notable reorientation of collagen fibres occurs, osteocytes seem wider than those situated at the base (Figure 12b). However, they predominantly maintain a spindle shape, with dendritic processes that project perpendicularly on the cell body and extend from their poles. Osteocyte long axis follows the orientation of the collagen fibres in the extracellular matrix. Osteocytes close to the border, where a shift in collagen fibre orientation occurs, occasionally exhibit irregular or more rounded morphology with less organized dendritic processes.

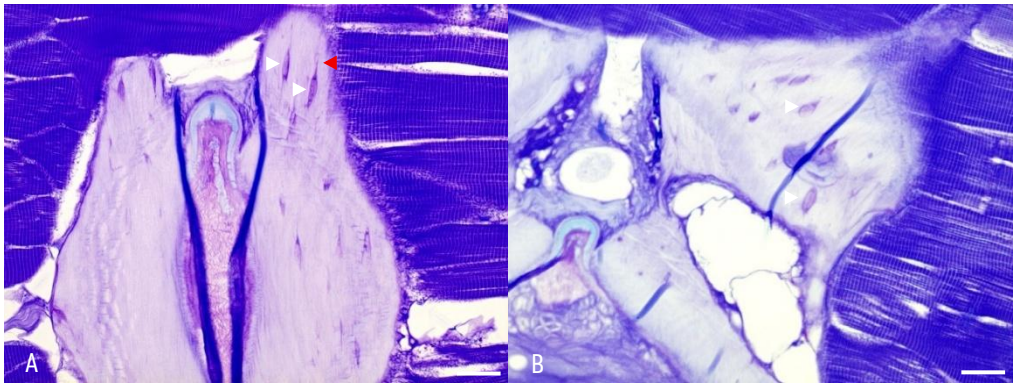

Figure 12: microscopy images of osteocytes in the neural base. (A) lateral attachment zone of the neural base with spindle shaped osteocytes (white filled arrows). Dichotomous branching observed in pole emanating dendrites (red filled arrow). (B) Part of the vertebra defined as the neural base with a 45 degree fibre angle. Spindle shaped wider osteocytes (white arrows, not all indicated in the picture to ensure visibility) (scale bar : 20 µm)

4.1.2.2 Neural Arch

In the neural arch base, osteocytes exhibit a wider, spindle-shaped morphology and are aligned with the orientation of the collagen fibres. Primary dendritic processes emanate from the poles as well as perpendicular from the osteocyte cell body. Branching occurs close to the primary dendrite base of the dendrites emanating from the cell body. Secondary dendrites, branch perpendicular on the primary dendrites and are following the orientation of the cell body axis. Dichotomous and trichotomous branching was observed. Tertiary dendrites were observed as well (Figure 13a). As the neural arch reduces in thickness, osteocytes become more elongated and thinner, still having the same dendritic characteristics (Figure 13a).

Osteocytes are uniformly distributed throughout the neural arch, extending from the deep bone matrix to the bone surface. As the neural arch terminates and transitions into the neural spine, where its left and right laminae fuse, we observe a series of smaller osteocytes with short dendritic processes orientated perpendicular to the neural spine orientation (Figure 13b).

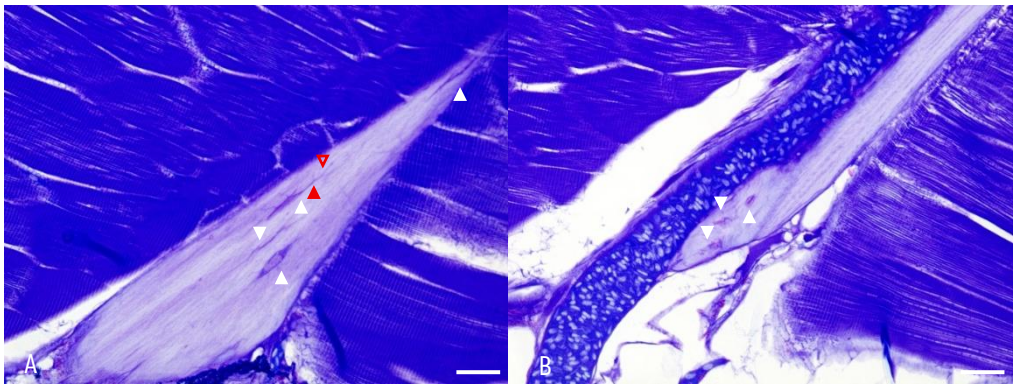

Figure 13. Microscopical images of the neural arch of caudal vertebrae of *Danio rerio*. (A) Spindle shaped osteocytes in the neural arch (White filled arrows). primary branching (leading to secondary dendrites; red filled arrow) and secondary branching (leading to tertiary dendrites; red hollow arrow) (B) Smaller outlines of osteocytes in the transitional region between neural arch and neural spine (white filled arrows). (scale bar: 20 µm)

4.1.2.3 Neural Spine

Osteocytes in the neural spines are typically flat and elongated, yet some small, flattened osteocytes are observed as well. Long dendritic processes extend from the cell poles, aligning with both the orientation of the cell body and the surrounding collagen fibres. These pole-extending dendrites undergo dichotomous branching. Dendritic processes are not observed to project perpendicularly from the central axis of the osteocyte body. Osteocytes are homogenously arranged in the Neural Spine (Figure 14).

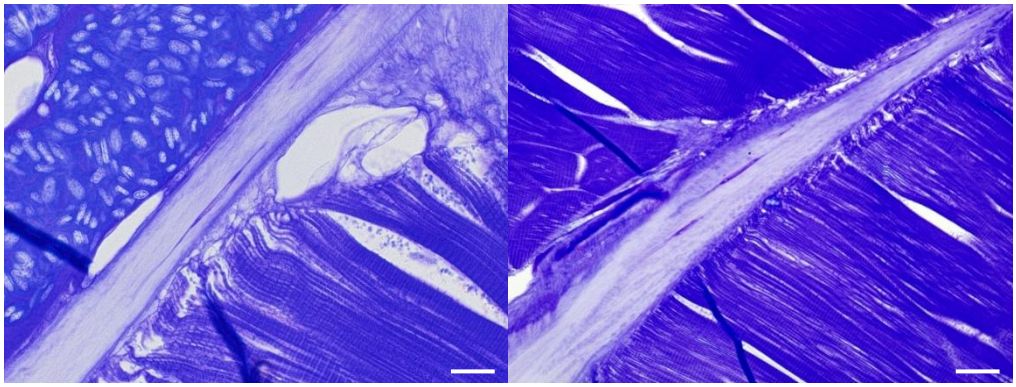

Figure 14. Microscopical images of osteocytes in the neural spine (scale bar: 20 µm).

4.1.3 Ventral outgrowth – Haemal Arch

Osteocytes are mostly spindle shaped in the haemal arch (Figure 15b). They have dendritic processes perpendicular on the cell body as well as dendritic processes extending from the poles following the orientation of the collagen fibres. Cell body extending osteocytes branch close to the base of the primary dendrite and secondary osteocytes are orientated following the collagen fibres. Dendritic arborization presented as either dichotomous or trichotomous branching events. Osteocytes are evenly distributed across the haemal arch. They appear to be arranged closer to each other compared to in other regions of the vertebrae (Figure 15). Osteocytes follow the orientation of the collagen fibres. However also irregular, rounder shaped osteocytes were observed in regions of less organized bone and newly constructed bone (Figure 15b).

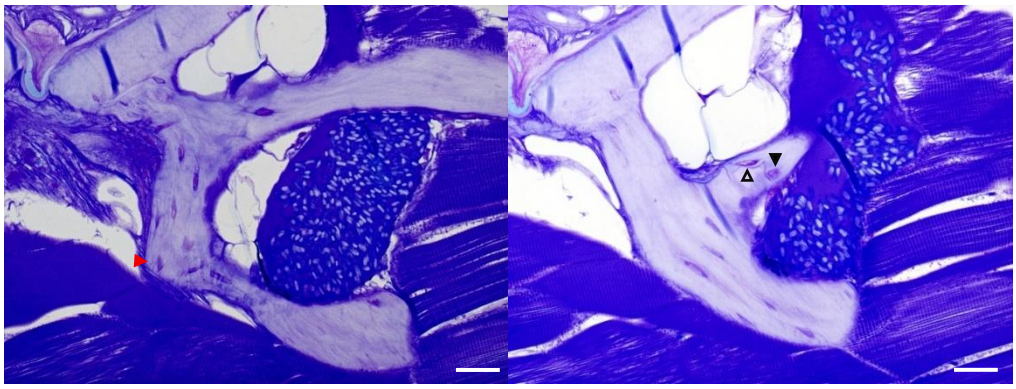

Figure 15. Microscopic images of osteocytes in the Haemal arch. A: osteocytes in high densities in the heamal arch Red filled arrow showing a trichomous primary branching of cell body emanating dendrites. B: osteocytes in the haemal arch with newly constructed bone encompassing a rounder (black filled arrow) and spindle shaped (black hollo arrow) osteocyte (scale bar: 20 µm).

4.1.4 Trabeculations

Polarized light microscopy revealed a difference in collagen fibre orientation between the trabeculations and the outer regions of the vertebral centrum (Figure 16b). The dorsal and ventral trabeculations appear to be mechanically supported by a trabecular beam oriented at approximately 45 degrees, which connects with the vertebral centrum (Figure 16a). Towards the mid-region of the vertebra, differentiating between the trabeculation and the vertebral centrum becomes difficult due to a change in the fibre orientation of the central part of the vertebral body, which exhibits a similar fibre alignment.

Osteocytes within the trabeculations are generally spindle-shaped, with dendritic processes extending from the poles and radiating perpendicular from the cell body. These osteocytes align with the orientation of the collagen fibres. Branching of perpendicular dendrites on cell body occurs dichotomously as well as trichotomous. Branching of pole-emanating dendrites was solely dichotomous. Dendritic processes radiating from the cell body branch close to the dendritic base, and secondary dendritic processes follow the orientation of the osteocyte body. Tertiary dendrites were also observed (Figure 16c, d, e, f). Some osteocytes appear rounder or irregular in shape and are observed both in newly constructed bone (Figure 16g) and in regions where the collagen fibre orientation shifts abruptly, such as at the attachment zone between the trabeculation and the centrum (Figure 16d & e).

There were no significant differences in osteocyte morphology or organization among the ventral, dorsal, and lateral trabeculations. However, the ventral and dorsal trabecular region were more extensively visible, which allowed for a clearer visualization of osteocyte shape, spatial distribution, and dendritic branching patterns. Osteocytes were evenly arranged, extending from the deep bone matrix to the bone surface.

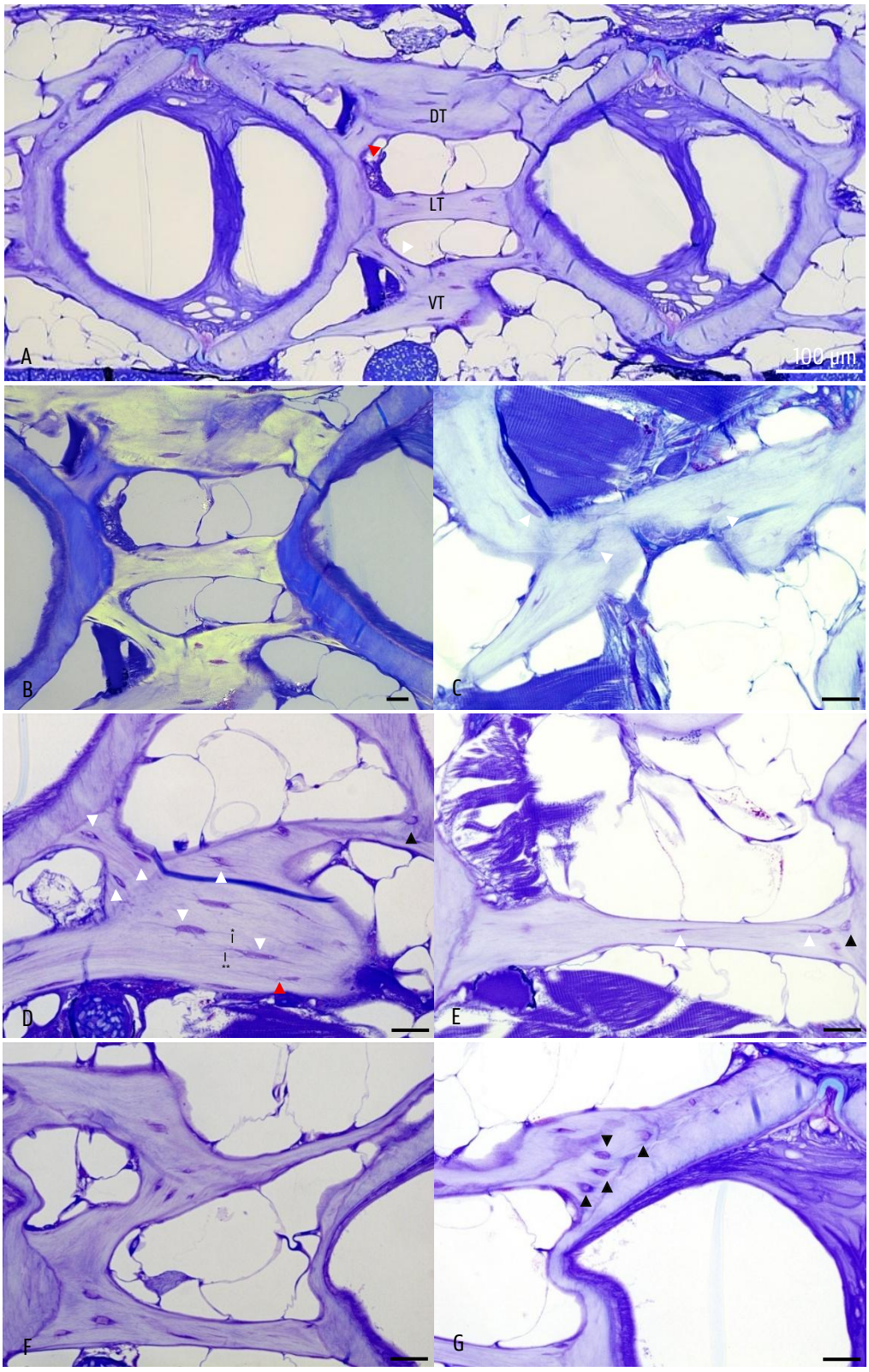

Figure 16 (Page 22) A: microscopical overview image of trabeculations in the caudal vertebrae, with dorsal trabeculation (DT), lateral trabeculation (LT), and ventral trabeculation (VT). Supporting beams of the dorsal and ventral trabeculations are indicated with a red resp. yellow arrow. B: polarized light microscopy showing the different orientations of collagen fibres of the trabeculations in comparison to the vertebral endplates. C: Dorsal trabeculation with spindle shaped osteocytes (white arrows) D: ventral trabeculation, with spindle shaped osteocytes (white filled arrows, not all indicated to assure visibility) and a round osteocytes (black filled arrow). Primary branching (*) and secondary branching (**) as well as trichotomous arborization (red filled arrow). E: lateral trabeculation with spindle shaped osteocytes (white filled arrows) and round osteocytes (black filled arrow). F: dorsal and lateral trabeculation connected with beam. G: Osteocytes in newly constructed bone (black filled arrows) between the dorsal trabeculation and posterior endplate. (scale bars B-G: 20 µm)

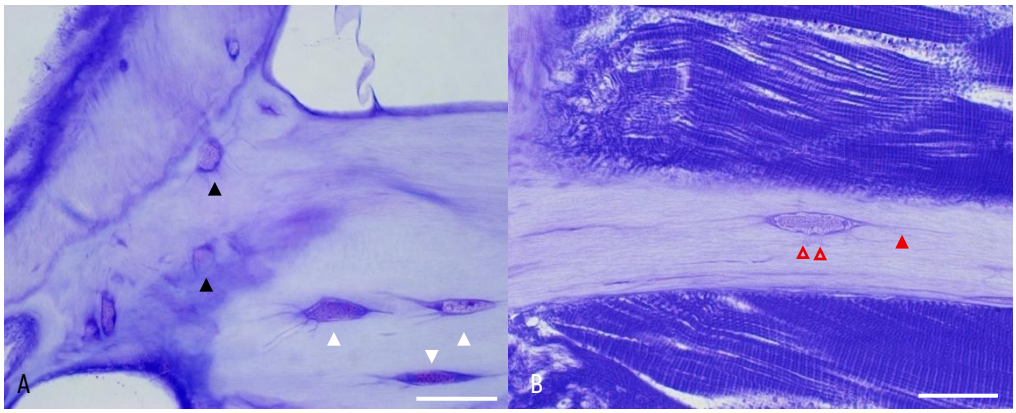

Figure 17. High magnification images of osteocytes in trabeculations; A: Ventral trabeculations with 2 clear distinct morphotypes. Rounder shaped osteocytes (black filled arrows) in region transitional region and in region with woven bone structure, ass well as spindle shaped osteocytes (white filled arrows). B: Osteocyte in lateral trabeculation. With clear pole emanating dendrites following the orientation of the collagen fibres (filled red arrow) and cell body emanating dendritic processes with a short perpendicular stem and dichotomous branching events (red hollow arrows) 5scale bars: 20 µm).

4.2 Quantitative study

We reconstructed 703 osteocytes located in within one hemi section of a zebrafish caudal vertebra. 4 consecutive sections were stained followed by 4 unstained sections. This methodology reconstructed approximately one quarter of the of the total vertebral column. Extrapolating this data gives an estimation of 2800 osteocytes located within a complete caudal vertebra of the Zebrafish.

4.2.1 Morphological features

4.2.1.1 Length

The measured osteocyte upper value lengths ranged from 6.114 µm to 38.575 µm. The boxplot of the length of osteocytes illustrates variation between and within the different regions of the vertebrae (Figure 18).

To determine if variation between regions is significant, we performed a Welch Anova as the assumption of homogeneity of variances was not met (Levene's test: pr (>F) = 0.003676**). The Welch Anova test is significant on the 0.05 significance level (p= 0.01456, F=4.0173).

To compare regional variation of osteocyte length we performed a Games Howell post hoc test. We observe a significant difference (p <0.05) between osteocytes located in the Neural spine (24.757 ± 5.673 µm) and the centrum (13.971 ± 5.017 µm, p = 0.0025), dorsal trabeculation (15.100 ± 6.270µm, p = 0.0067), haemal arch (13.856 ± 4,109 µm, p = 0.0023) (Table 2). We also observe a significant difference between lengths between centrum and the ventral trabeculation (p= 0.0172). There is no p values calculated for difference in C-NB and NB between other regions as there are to little osteocytes found that show their full length (N=2) (Appendix: Table 4).

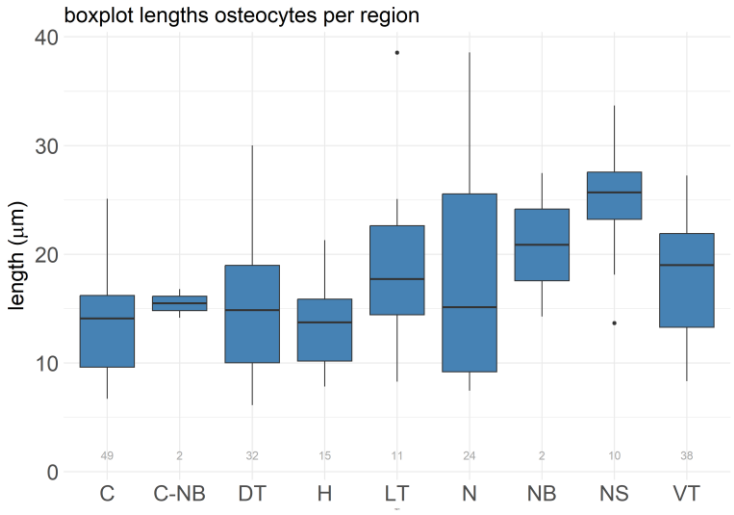

Figure 18. Boxplot showing the distribution of osteocyte lengths across different regions of the vertebrae, based on osteocytes that were deemed acceptably measured (grey numbers, Total 183). (C: Centrum (endplates+ vertebral body), C-NB: transition centrum and neural base, DT: dorsal trabeculation, H: haemal arch, LT: lateral trabeculation, N: neural arch, NB: neural base, NS: neural spine, VT: ventral trabeculation)

4.2.1.2 Diameter

The measured osteocyte upper value diameter ranged from 1.383 µm to 9.352 µm. Boxplot on the diameter of osteocytes illustrates less variation between different regions of the vertebrae, however we observe a reduction in diameter in the neural spine osteocytes (Figure 19).

To determine if variation between regions is significant, we performed an ANOVA (assumptions were met: Shapiro wilk : W = 0.96257, p-value = 8.631e-08; Levene's Test: F value = 2.9864, Pr(>F) = 0.003676). The Anova showed a significant regional difference (p=0.000475***, F-value: 3.615) in diameter. To compare regional variation of osteocyte diameter we performed a Bonferroni post hoc analysis. We observe a significant difference (p <0.05) between osteocytes diameter located in the neural spine (2.643 ± 1.096µm) and the centrum (4.240 ± 1.273 µm, p = 0.0020), dorsal trabeculation (4.123 ± 1.459 µm, p = 0.0117), haemal arch (4.260 ± 1.628 µm, p=0.0069), lateral trabeculation (4.184 ± 1.569 µm, p=0.0246), neural arch (4.035 ± 1.485 µm, p= 0.0443), and ventral trabeculation (4.721 ± 1.524 µm, p = 0.000) (Table 2, Appendix: Table 5).

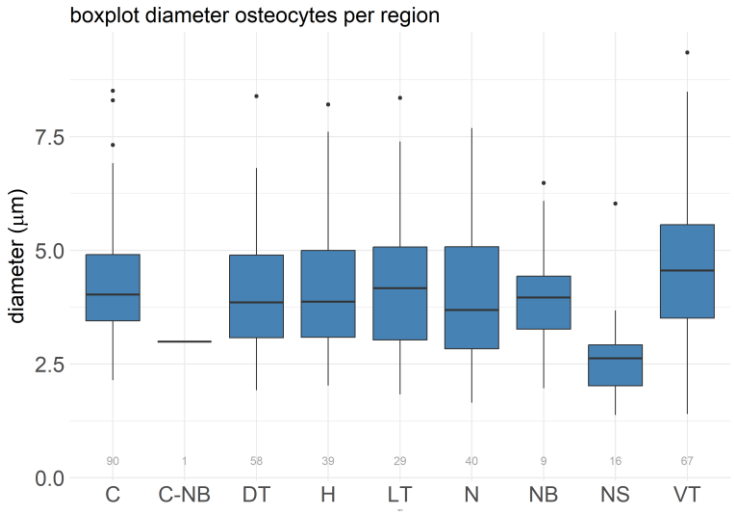

Figure 19. Boxplot showing the distribution of osteocyte diameter across different regions of the vertebrae, based on osteocytes that were deemed acceptably measured (grey numbers, Total: 349). (C: Centrum (endplates+ vertebral body), C-NB: transition centrum and neural base, DT: dorsal trabeculation, H: haemal arch, LT: lateral trabeculation, N: neural arch, NB: neural base, NS: neural spine, VT: ventral trabeculation)

4.2.1.3 Length: Diameter Ratio

The ratio of the osteocyte length to diameter gives insights on the three-dimensional morphology of the osteocytes (Figure 20). A ratio closer to zero indicates a more spherical shape. Higher ratios indicate greater lengths and/or lower diameters characterized by a spindle shaped elongated morphology. The boxplot illustrates a higher length diameter ratio in the Neural Spine.

To determine if there is significant variation between different regions of the vertebrae we perform a Kruskal Wallis analyse as both assumptions for normality and homogeneity of variances is not met (Shapiro Wilk test: p = 0.003743, Levene's test : pr(>F) = 5.64e-6). A significant p-value of 3.289e-5 was found, meaning there is variation in ratio between regions. We performed Dunn's test for pairwise multiple comparisons of mean regional osteocyte length/diameter ratios. We observe a significant difference (p <0.05) between osteocytes located in the neural spine and the centrum (p = 5.403e-6), Dorsal Trabeculation (p = 4.938e-3), Haemal arch (p=3.846e-2), Neural Arch (p= 3.979e-2), Ventral Trabeculation (p = 9.851e-4) (appendix: Table 7).

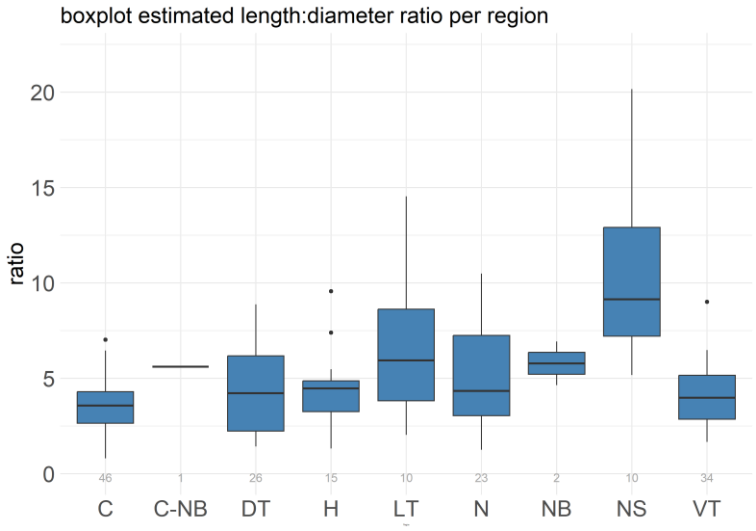

Figure 20. Boxplot showing the distribution of osteocyte length: diameter ratio across different regions of the vertebrae, based on osteocytes that were deemed acceptably measured (grey numbers, Total: 167). (C: Centrum (endplates+ vertebral body), C-NB: transition centrum and neural base, DT: dorsal trabeculation, H: haemal arch, LT: lateral trabeculation, N: neural arch, NB: neural base, NS: neural spine, VT: ventral trabeculation)

4.2.1.4 Volume

The measured osteocyte volume ranged from 131,875 to 5339, 562 μm^3. The Boxplot on the volume of osteocytes shows some variation between region of the vertebra (Figure 21).

To determine if variation between regions is significant, we performed a Kruskal Wallis test as the assumption for normality was nit met (Shapiro: w= 0,89361; p-value = 1,371e-9). Variances were equally distributed (Levene's test: F: 1.2425, pr(<F) = 0.2778). The Kruskal Wallis test has a p-value of 0.0029 and as such significant on the 0.05 significance level. (Chi squared = 23,66), meaning at least one region has different median estimated osteocyte volume from the rest. To compare regional variation, we performed a Dunn post hoc analysis, showing significant adjusted P values when comparing the ventral trabeculation with the Haemal arch (p-adjusted: 0,0019), neural arch (p-adjusted: 0,0088) and neural spine (p-adjusted: 0,044) osteocyte volumes (Appendix: Table 6).

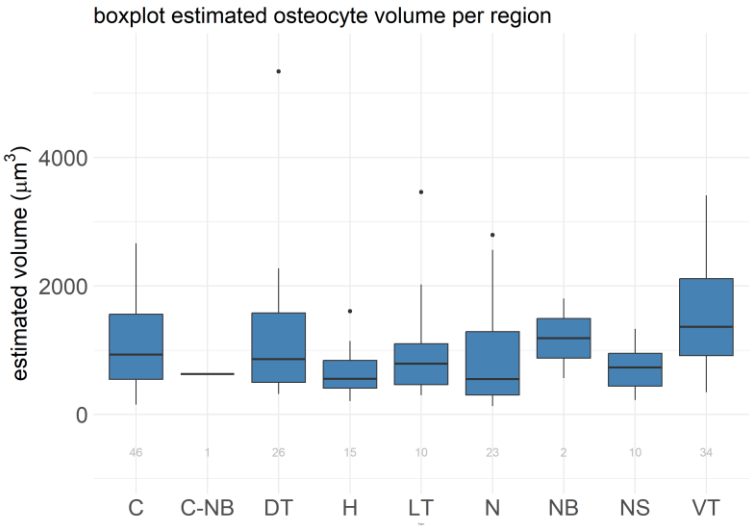

Figure 21. Boxplot showing the distribution of osteocyte volume: diameter ratio across different regions of the vertebrae, based on osteocytes that were deemed acceptably measured (Grey numbers, Total: 167).(C: Centrum (endplates+ vertebral body), C-NB: transition centrum and neural base, DT: dorsal trabeculation, H: haemal arch, LT: lateral trabeculation, N: neural arch, NB: neural base, NS: neural spine, VT: ventral trabeculation)

Table 2. Mean and standard deviation of osteocyte quantitative traits across different regions of the caudal vertebra. (C: Centrum (endplates+ vertebral body), C-NB: transition centrum and neural base, DT: dorsal trabeculation, H: haemal arch, LT: lateral trabeculation, N: neural arch, NB: neural base, NS: neural spine, VT: ventral trabeculation)

Region	Mean length µm	SD Length µm	Mean Diameter µm	SD Diameter µm	Mean Volume µm³	SD Volume µm³
C	13,971	5,017	4,240	1,273	1.112,150	675,881
C-NB	15,478	1,870	2,992	NA	629,972	NA
DT	15,100	6,270	4,123	1,459	1.150,048	1.045,244
H	13,856	4,109	4,260	1,628	664,173	378,249
LT	19,011	8,252	4,184	1,569	1.085,935	975,625
N	17,141	9,096	4,035	1,485	933,145	813,364
NB	20,862	9,327	4,091	1,433	1.185,052	877,289
NS	24,757	5,673	2,643	1,096	707,670	359,633
VT	17,970	5,320	4,721	1,524	1.589,143	844,037

4.2.1.5 Density

Density of the regions in the bone were analysed and summarized in Table 3. The neural spine had the overall lowest cellularity of 201,51 cells/mm² while the Haemal Arch had the highest cellularity with 650,14 cells/mm². Due to lack of replicates, no further statistical analyses can be done with these data.

Table 3. Total area of observed vertebral region and number of osteocytes counted within. Resulting in an estimation of the amount of cellularity of bone in each region. (C: Centrum (endplates+ vertebral body), DT: dorsal trabeculation, H: haemal arch, LT: lateral trabeculation, N: neural arch, NB: neural base, NS: neural spine, VT: ventral trabeculation)

	C	**NB**	**N**	**NS**	**DT**	**LT**	**VT**	**H**
Area (µm²)	2,272E+6	1,200E+5	2,784E+05	1,687E+05	4,367E+05	1,709E+05	4,867E+05	1,661E+05
Amount of osteocytes	323	15	58	17	99	45	93	54
density (cells/mm²)	284,28	250,01	416,74	201,51	453,39	526,47	382,18	650,14

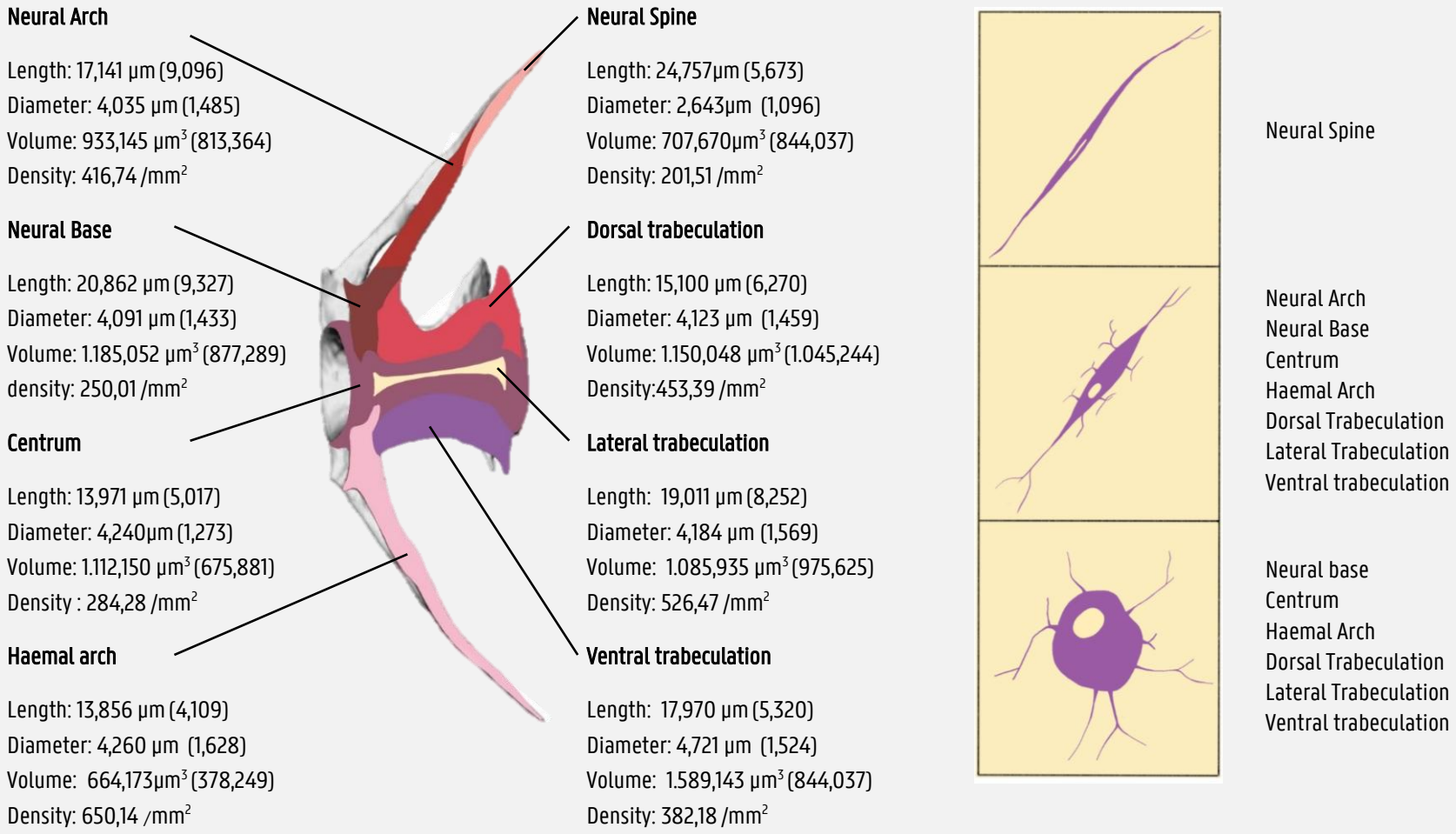

Figure 22. Overview of reconstructed osteocytes in different regions of the caudal vertebrae of Danio rerio : (left) caudal vertebra: regions that are studied have different colours. regions name indicated in bold letters. Length, diameter, volume and density of osteocytes in each region indicated (standard deviation between brackets). (right): schematic drawing of key osteocyte morphologies found in different regions of the caudal vertebra.

5 Discussion

This study investigated the morphological features and spatial distribution of osteocytes in zebrafish caudal vertebrae, a subject previously understudied due to the late ontogenetic appearance of these cells (Huysseune, 2000). We identified three distinct osteocyte morphologies embedded within the collagen matrix. Two of these morphologies, consistent with previously described Type I and Type II osteocytes (Bonucci, 2009; Haridy et al., 2021; Kerschnitzki et al., 2011; Totland et al., 2011; Weigele & Franz-Odendaal, 2016), were observed throughout all but one vertebral region. The third, morphologically distinct cell type was found exclusively within the neural spine. A functional lacuno-canalicular network was inferred from the observation of a vast, organized and connective dendritic network, with high osteocyte densities across all regions of the vertebra, this challenges the statement of a poorly developed osteocyte lacuno-canalicular system in zebrafish bones by Cao et al. (2011). Furthermore, regional differences in osteocyte density were observed. An overview of these combined results is presented in Figure 22.

5.1 Morphology

Osteocytes vary in morphology within and between distinct regions of the vertebra. This osteocytic variation on different scales corroborate the results of research by Haridy et al. (2021). Based on our measurements, osteocytes across the entire vertebra ranged in length from 6.114 to 38.575 µm, in diameter from 1.383 to 9.352 µm, and in volume from 131.875 to 5339.562 μm^3. Notably, the calculated osteocyte volumes in this study are significantly higher than those reported in previous research. With a mean value of 1122.467 ± 820.760 μm^3, our calculations showed osteocytes more than 10 times the volume observed micro CT-based study by Suniaga et al. (2018)(V = 77.6 ± 10.3 μm^3). Although high resolution micro CT can provide a 3D image, osteocytes structures are below the resolution threshold of micro CT (Kague et al., 2024) and thus artefacts are generated that possibly explain the differences in osteocyte volume measurement between this study and the study by Suniaga et al. (2018). Theoretically, assuming that osteocytes are ellipsoid and not flattened or irregularly shaped could lead to an overestimation of the osteocyte volumes when using length and diameter to calculate their volumes. There are, however, no indications from literature that osteocytes are not spindle shaped. Mice lacunar diameters of 15-20 µm (Moharrer & Boerckel, 2021), indicate a slightly reduced osteocytes diameter in zebrafish bone. This was to be expected due to the smaller genome size in zebrafish and the general correlation between genome size (total amount of nuclear DNA) and cell size (Witten et al., 2017).

5.1.1 Osteocyte morphology relates to collagen fibre arrangement

Our findings align with our initial hypothesis that bone typology significantly influences osteocyte shape and the orientation of both the cell body and dendritic processes within zebrafish vertebrae. Specifically, a direct relationship between osteocyte morphology and the orientation of collagen fibres in the surrounding bone matrix was observed. This observation supports the expectation that osteocytes exhibit a close alignment with collagen fibres in organized bone, while demonstrating a less pronounced alignment in woven bone.

1. Two primary osteocyte morphologies, Type I and Type II, were observed, consistent with descriptions of other studies (Bonucci, 2009; Davesne et al., 2020a; Kerschnitzki et al., 2011; Totland et al., 2011; Weigele & Franz-Odendaal, 2016). Additionally, some transitional cell shapes were identified. Clearly, not all osteocytes can be neatly categorized into a single morphology (Figure 23). Veno et al. (2006) have shown the dynamic nature of osteocytes and their cell processes (Bonewald & Johnson, 2008). Cell bodies can undergo deformations. Consequently, transitional forms can be explained as snapshots (Shiflett et al., 2019), as such redirecting signals from the cell body and the dendrites in the ECM (Bonewald & Johnson, 2008). Spindle-shaped osteocytes were most common. Their long axis follows the orientation of the surrounding collagen fibres. Transverse sections of

these cells showed an almost round outline at the endplates, indicating that the cells are not flattened. In contrast, spherical osteocytes were sporadically observed in specific regions of the bone. Their presence was noted in transitional zones, such as at the interfaces between different vertebral elements where type I collagen fibres show an abrupt change in orientation, as well as in areas of new bone formation. This observation largely aligns with the hypothesis by (Haridy et al., 2021) that osteocyte shape is related to bone type. They proposed that lacunae in organized (e.g., lamellar or parallel-fibered) bone being more elongate and regularly shaped than those in woven bone. The presence of rounder osteocytes in newly formed bone (i.e. primary woven bone) is consistent with their findings. However, the sporadic observation of rounder osteocytes within organized (lamellar) bone, specifically in transitional zones where an abrupt change in the orientation of collagen fibres occurs, suggests that osteocyte morphology is not solely determined by the general bone type, but local bone architecture may play a role to the mechanical environment of the bone and thus influences osteocyte shape. Collagen assembly dynamics was shown in previous studies by Shiflett et al. (2019) and others. Filament ECM motion are moved by large scale tissue layers during embryonic morphogenesis, this could explain the spatial distribution of type I osteocytes in in transitional zones.

2. The orientation of dendritic processes differs between the two osteocyte morphotypes. In spherical osteocytes, dendrites radiate omnidirectional from the cell body. The primary dendritic processes of elongate osteocytes have a highly polarized orientation. They extend from the cell poles, following the orientation of its long axis and, consequently, the surrounding collagen fibres as well as perpendicularly on the cell body. This pattern of primary dendritic processes, emanating from two predominant directions on the cell body, aligns with the directionality analyses conducted by (Haridy et al., 2021) on fossil placoderm fish. A similar orientation was described by (Bonucci, 2009) in studies of human bone. Secondary dendrites tend to follow the orientation of the collagen fibres after branching.

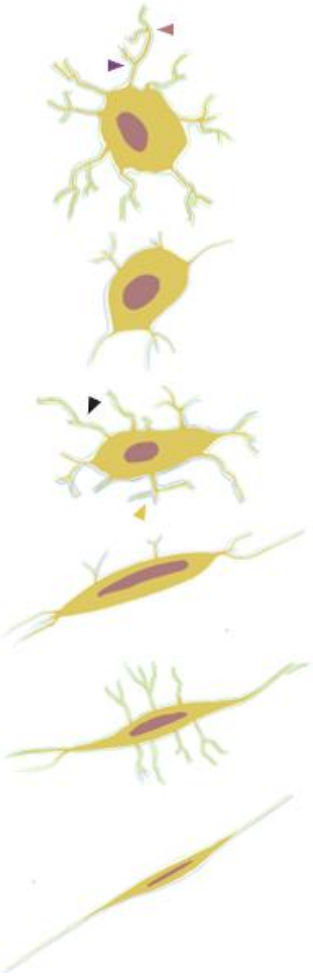

Figure 23. Schematic drawings of different osteocyte shapes that are present in Danio rerio vertebrae. From rounder shaped osteocyte cell bodies to extremely elongated cell bodies. Purple arrow: primary branching ; Pink arrow: secondary branching; Black arrow: node degree of 3; Yellow arrow: node degree of 4.

5.1.2 Osteocyte morphology differs between vertebral body elements

We hypothesized that osteocyte volume and shape would vary between distinct vertebral regions, and that this variation would correlate with differences in bone matrix volume and mechanical loading, a relationship suggested by Huysseune (2000).

1. Significant regional differences in osteocyte morphology and orientation were found within the vertebra, particularly in the neural spine. These cells are extremely elongated and spindle-shaped, with a mean length of 24.757 µm (±5.673 µm), diameter of 2.643 µm (±1.096 µm), a volume of 707.670 µm (±359.633 µm). Unlike other spindle-shaped osteocytes, the dendritic processes of these cells extend only from their poles, following the alignment of extracellular collagen fibres. The neural spine develops as a single median extension from the neural arch (Bird & Mabee, 2003). The neural arch has a protective function encompassing the neural tube, while the neural spine has only a mechanical function as muscle attachment. Thus, one potential explanation is the

higher mechanical loading on the neural spine due to extensive muscle attachment. The striking similarity between these neural spine osteocytes and those found in intermuscular bones (i.e. ossified myoseptal tendons) suggests a possible link between osteocyte shape and specific high mechanical demands of the surrounding tissue (Hall, 2015; Lyall et al., 2024; Nie et al., 2022). However, it remains a possibility that osteocyte morphology is influenced by other factors, such as the low bone matrix volume (Huysseune, 2000) found in both the spine and intermuscular bones.

2. Additionally, significant regional differences in osteocyte morphology and volume were observed. The ventral trabeculation showed a significant difference in osteocyte length when compared to the centrum. Moreover, its osteocyte volume was significantly different from both the neural arch and the haemal arch. These observed differences may be partly attributed to our sectioning methodology. For instance, the concentric collagen fibre orientation in the outer part of the centrum (including the endplates) (Kague et al., 2021) often caused osteocytes to be sectioned at an oblique angle, resulting in incomplete or ellipsoid outlines. Although these sections were labelled as complete (as a perfect outline of the cell was visible), the measured length was consequently an underestimate. A similar effect due to shifted orientation relative to the cutting plane may have also influenced volume measurements in the neural and haemal arches. While the measured diameter from these sections is a good indicator of the osteocyte's true diameter. Aside from these specific regional comparisons, no other significant morphological differences were observed within the vertebra.

5.2 Lacuno-canalicular network

In contrast to the findings of Cao et al. (2011), This study reveals a vast and highly organized osteocyte network within the vertebrae of *Danio rerio*, an observation that aligns with the work of several other studies (Davesne et al., 2020a; Kague et al., 2021; Ofer et al., 2019). The complete caudal vertebra contains an estimated 2800 osteocytes. The network is characterized by extensive dendritic arborization and high osteocyte densities. These densities were further demonstrated to be heterogeneous, exhibiting significant variation both between and within specific vertebral regions.

5.2.1 Densities

1. Our findings reveal distinct patterns in osteocyte density across the vertebra regions. The neural and haemal arch exhibited the highest osteocyte densities, followed by trabeculations. In contrast, the neural base, neural spine and centrum displayed the lowest densities. This differential distribution aligns with the biomechanical analyses by Ofer et al. (2019), where the FEA simulation found highest strains at distal parts of the trabeculations and at the neural and haemal arch. The strong correlation between regions of high mechanical strain and high osteocyte density in our observations suggests a mechanosensitive response of the osteocyte population. This hypothesis is supported by the findings of Totland et al. (2011)who observed an increase in osteocyte densities in exercised salmon. Indicating a possible increase in osteocyte densities with increases mechanical loading. However, due to the absence of replicates in the statistical analyses in densities between region, further research is necessary to validate these results. Interestingly, an exception to this pattern is the neural spine. Despite being a mechanically loaded region, it exhibited a low osteocyte density, which contradicts the earlier hypothesis. This finding may be explained by an alternative mechanism of load perception. Atkins et al. (2015) found increased bone material stiffness in anosteocytic loaded bones of Tilapia and research on salmon showed an increase in mineral content in bone with higher mechanical loading (Totland et al., 2011). They propose that the hypomineralized collagen bundles participate in mechanotransduction and load perception by bone lining osteoblasts (Tauer et al., 2024). This suggests that an alternative mechanism for mechanotransduction may exists (Haridy et al., 2021; Witten & Huysseune, 2009). Because the low bone matrix volume of the thin neural spine, spatial restraints cause a lower osteocyte density. Ofer et al. (2019) observed high SOST-positive expression cells (i.e osteoblasts) on the surface

of the neural spine in medaka and similar expression in Zebrafish. They hypothesize that SOST has a regulatory role in modeling of the anosteocytic skeleton. As the bone matrix volume of the neural spine is low in contrast with the bone outer surface, we hypothesize that part of the mechanosensing and transduction can be fulfilled by the osteoblasts and bone lining cells (Bonewald & Johnson, 2008). Further research should investigate whether this poorly developed lacuno-canalicular network in neural spines is counteracted by ECM composition or SOSt-positive osteoblast on the surface of the bone matrix volume in the neural spine.

2. Additionally, beyond the regional variations, a heterogeneous distribution of osteocytes was observed within the regions, particularly in the centrum. Within the vertebral body endplates and cone regions, osteocytes are clustered in close proximity to the Sharpey Fibres. Sharpey Fibres are bundles of collagenous fibres that continue from the periosteum, effectively embedding the ligament in the bone (Hall, 2015; Moss, 1961). The Sharpey Fibres observed in the endplates are originating from the intervertebral ligament. These unmineralized fibres are sensitive to mechanical stresses and constantly triggered due to swimming behaviour of the fish. This further reinforces the hypothesis that osteocyte distribution and density is intricately linked to localized mechanical loading. Hall (2015) highlighted the challenges associated with maintaining attachment sites during the developmental growth of bone and muscle. Furthermore, Witten & Hall (2003) demonstrated that a reduction in mechanical loading can trigger the resorption of both skeletal tissue and Sharpey's fibres. These findings suggest that osteocytes may be necessary to guide bone growth and remodelling, thereby preserving the integrity of the undulating system.

5.2.2 Dendritic processes

The morphology and connectivity of osteocyte dendritic processes is a key characteristic of the lacuna-canalicular network. We observed variations in the orientation of dendritic processes between round and spindle-shaped osteocytes with two predominant directions in the spindle shaped osteocytes and random orientation in the rounder osteocytes.

1. We identified primary, secondary, and tertiary dendrites, with branching occurring dichotomously or trichotomously. The overall amount of branching appeared lower than that reported in mammalian species such as mouse (more than 4 branching events in *Mus musculus* and *B. trautscholdi* (Buenzli & Sims, 2015; Haridy et al., 2021). This could be attributed to methodological limitations, potentially underestimating the true complexity of the dendritic network as higher branching classifications are reducing in dendritic thickness and as such higher resolution is needed. A particularly striking observation was the organized dendritic network clearly visible at lateral sections of the periphery, showing an extensive number of "free" dendrites (i.e. dendrites origin is not traceable in the image) oriented perpendicularly to Sharpey's fibres. This perpendicular orientation is highly suggestive of a specialized arrangement of spindle shaped dendrites, which suggests a functional network constructed by these spindle shaped osteocytes in contrast to the under established network in Salmon bone observed by (Totland et al., 2011) . These fibres, sensitive to mechanical stress (Hall, 2015; Moss, 1961), are being surrounded by high density of dendritic processes. This strengthens the hypothesis of the mechanosensory role of osteocytes and their dendrites in these critical load-bearing regions.

2. The observation of dendritic connections of round osteocytes over regions, in combination with the highly organized network of dendrites of spindle shaped osteocytes within the regions, indicates a vast continuum and functional lacuna-canalicular network throughout the vertebrae of *Danio rerio,* in contrast to the observation of Cao et al. (2011) .

5.3 Limitations

The quantitative analysis of osteocytes was limited by a small sample size, which may impact the statistical power and generalizability of the findings. Specifically, osteocytes were only observed in three caudal vertebrae from a single zebrafish, and quantitative analysis was performed on just one of these vertebrae. To ensure statistically robust results, future studies should analyse a larger sample, including multiple vertebrae from several individuals.

A significant methodological challenge was distinguishing between bone regions. For example, the neural base, neural arch, and dorsal trabeculation appeared as a continuous structure in microscopic images, with no clear transitional zones. While we made our best efforts to define these regions for reproducibility, this ambiguity may introduce some degree of measurement error. Future research would benefit from using 3D reconstruction techniques or performing a regional dissection to analyse these bone regions separately, thereby allowing for a more precise and accurate evaluation of osteocyte distribution.

Our analysis of osteocyte morphology was based exclusively on parasagittal sections of the vertebrae, which provided a two-dimensional view. This approach necessitated assumptions about the full three-dimensional morphology and distribution of osteocytes, possibly leading to an overestimation of the osteocyte volume. A more comprehensive understanding would require a multi-planar approach. Davesne et al. (2020a) also mentioned the limiting ability to characterize and quantify three dimensional structures of the lacunae of osteocytes using ground or thin sections. To overcome this limitation, future studies could integrate a combination of parasagittal and transverse sectioning. This would allow for a more complete reconstruction of the cellular network. Alternatively, advanced imaging techniques such as 3D Raman microscopy or synchrotron microtomography offer powerful, non-destructive methods for in-situ 3D analysis. These approaches however risk losing the benefits of discriminating bone types according to their structure and orientation of the collagen fibres (Davesne et al., 2020a)

6 Conclusion

The limited description and understanding of osteocytes in the zebrafish, one of the most used model organism in biomedical research, presents a significant knowledge gap. Addressing and closing this gap is critical for enhancing the utility of zebrafish in developing therapeutic interventions for skeletal diseases. A deeper comprehension of zebrafish osteocyte biology can increase the value of zebrafish model for the study of human bone diseases, particularly bone loss, in aging population. Contrasting hypotheses exist regarding the strength of the lacuno-canalicular network in zebrafish bones. Our study showed an extensive lacuno-canalicular network which functionality (as a mechanosensing organ) is inferred from high overall densities of the osteocytes in the vertebra. Heterogeneous osteocyte densities within (clearly visible as concentration of osteocytes around the Sharpey fibres in the vertebral endplates) and between different regions are linked to differences in the mechanical functions of regions of the vertebra. This finding strengthens the use of zebrafish as a model for understanding how moderate mechanical loading, which is known to maintain healthy bones in mammals, affects bone structure. Additionally, our research reveals that zebrafish osteocyte morphology is remarkably similar to that of mammals, with specific morphologies correlating with the orientation of collagen fibres and the mechanical environment of the extracellular matrix. However, a key question remains regarding the distinct morphological differences in osteocytes within the neural spine's ECM. We propose a hypothesis that the low bone matrix volume in this region, relative to its outer surface, may diminish the need for an extensive dendritic network, given the known mechanosensory role of bone-lining cells. Future research should focus on validating this hypothesis by investigating the precise relationship between bone matrix volume and osteocyte network complexity.

7 Summary

7.1 English

Francis Hamilton discovered one of the most important laboratory animals for studying vertebrate development: the zebrafish (*Danio rerio*). Zebrafish offer many advantages, including transparent embryos, external fertilization, rapid development, and high fecundity (Buenzli & Sims, 2015; Foessl et al., 2021; Kague & Karasik, 2022). These characteristics established them as a valuable model organism. More importantly, Moss (1961) discovered that zebrafish possess cellular bones, meaning their bones contain osteocytes. Osteocytes are the most abundant bone cells in the mammalian skeleton(Bonewald, 2011; Kague & Karasik, 2022). Dendritic processes from these cells crawl through the extracellular matrix of the bone in canaliculi (Bonewald, 2010, 2011; Franz-Odendaal et al., 2006). Together with the cell bodies that reside in lacunae, osteocytes form a lacuno-canalicular network (Buenzli & Sims, 2015). For a long time, little was known about these cells, as they were viewed as quiescent cells within the bone matrix. However, their crucial function as mechanosensors and transducers in mammalian bone has since been discovered, leading to a increase of studies on their role in healthy bone and their importance in bone diseases (Bonewald, 2010, 2011; Kague & Karasik, 2022; Tonelli et al., 2020).

Despite their use as a model organism, little is known about osteocytes in zebrafish bone. This is partly due to their late ontogenetic occurrence in the development of the skeleton (Huysseune, 2000; Witten & Huysseune, 2009). Some studies even suggested that zebrafish bones are acellular (Weigele & Franz-Odendaal, 2016), and others proposed an underdeveloped lacunocanalicular network (Cao et al., 2011), which is essential for osteocyte function. Given the increasing use of zebrafish in biomedical bone research and drug testing, it is critical to clarify the functionality of their osteocytes and their network.

A fine description of the osteocyte morphology in the zebrafish skeleton is the first step toward bridging this research gap. This study investigates the distribution and morphological characteristics of osteocytes in zebrafish vertebrae, with a primary focus on their shape, size, and the structure of their lacuna-canalicular network. The research aims to understand the relationship between osteocyte morphology and the surrounding collagen fibre arrangement. Based on existing literature, the study hypothesizes that osteocyte shape and density are influenced by bone typology and mechanical loading, and that zebrafish possess a poorly developed dendritic branching network. A fine description of the osteocyte morphology in the zebrafish skeleton is the first step toward bridging this research gap. By better understanding these cells, we can ensure the efficient use of zebrafish as a model organism and improve the effectiveness of drug testing.

This research was conducted by examining the osteocyte population within the caudal vertebrae of zebrafish, a skeletal element chosen for its dynamic mechanical environment. The vertebrae, composed of a vertebral body, neural and haemal arches, spines, and dorsal, ventral, and lateral trabecular plates, offer distinct mechanically different regions for analysis.

To characterize the osteocytes, we employed histology with both light microscopy and polarized light microscopy. This approach was selected due to the established correlation between collagen fibre orientation and the long axis of osteocytes, a relationship best visualized under polarized light. We performed both quantitative and qualitative analyses on osteocytes from each vertebral region. Our qualitative analysis focused on osteocyte morphology, which was reconstructed by measuring the cell's length and diameter in Fiji. For the quantitative analysis, we determined osteocyte density (cellularity) by counting the number of osteocytes in each region and dividing it by the total area examined. Statistical comparisons of osteocyte morphology across different vertebral regions were conducted using an ANOVA followed by post hoc analyses to identify significant differences.

Our measurements revealed that osteocytes throughout the entire vertebra exhibited a length ranging from 6.114 to 38.575 µm and a diameter ranging from 1.383 to 9.352 µm. We observed osteocyte variation at different scales, with significant morphological differences both within and between vertebral regions. Two main osteocyte morphologies were identified in all regions except for the neural spine. (i) Round to irregularly shaped osteocytes: These cells possessed dendritic processes radiating in all directions and lacked a specific orientation. They were typically found in newly formed bone and transitional zones where two regions, with either similar or different fibre orientations, converged. (ii) Spindle-shaped osteocytes: These cells had dendritic processes extending in two perpendicular directions. Their long axes generally followed the direction of the collagen fibres. A unique population of very thin, elongated osteocytes was found in the neural spine. These cells had a mean length of 24.757 µm (±5.673 µm) and a mean diameter of 2.643 µm (±1.096 µm), making them significantly different from osteocytes in other regions. Notably, these cells lacked dendritic processes emanating from the cell body, and the neural spine itself exhibited low cellularity.

We also observed significant differences in osteocyte densities across and within the vertebral regions. The highest densities were found in the neural and haemal arches, followed by the trabecular plates. Conversely, the centrum, neural spine, and neural base showed lower densities. An interesting finding was the high density of both osteocyte cell bodies and their dendritic processes in the endplates, specifically those perpendicular to the Sharpey fibres. This heterogeneity in osteocyte density within the vertebral body suggests a localized response to the mechanical environment.

The study's findings support the initial hypothesis that the type of bone significantly influences the morphology and orientation of osteocytes in zebrafish vertebrae. There is a clear link between osteocyte shape and the orientation of collagen fibres in the surrounding bone matrix. In organized (lamellar) bone, osteocytes and their dendritic processes show a strong alignment with the collagen fibres. Conversely, this alignment is less pronounced in woven bone.

While the general bone type is a major factor, the study suggests that local bone architecture and mechanical loading also play a crucial role. For example, the presence of rounder osteocytes in organized bone, specifically in transitional zones where collagen fibre orientation changes abruptly, points to the influence of the immediate mechanical environment. A striking similarity was observed between osteocytes in the neural spine and those in intermuscular bones. This is particularly interesting because both areas are subject to high mechanical demands, such as extensive muscle attachment (Hall, 2015; Lyall et al., 2024; Nie et al., 2022). This observation suggests that specific high mechanical forces may directly influence osteocyte shape. However, the text also offers an alternative explanation: the low bone matrix volume found in these areas could also be a contributing factor.

In contrast to some previous studies, this research reveals a vast and highly organized osteocyte network within the vertebrae of the zebrafish (*Danio rerio*), which aligns with the findings of other recent studies. The study also found a strong correlation between areas of high mechanical strain and high osteocyte density, suggesting that osteocytes are mechanosensitive. This idea is further supported by the heterogeneous distribution of osteocytes, particularly in the centrum where they are clustered near Sharpey's fibres (i.e. structures that anchor muscle to bone)(Hall, 2015; Moss, 1961; Witten & Hall, 2003). This localized clustering provides further evidence that osteocyte distribution is intricately linked to areas of high mechanical loading.

A significant knowledge gap exists regarding zebrafish osteocytes, hindering their use in skeletal disease research. Our study found an extensive, mechanosensitive osteocyte network in zebrafish vertebrae. Osteocyte density and distribution vary with mechanical loading, suggesting the fish is a strong model for studying how moderate forces maintain bone health. Zebrafish osteocyte morphology is similar to that of mammals, with cell shape correlating to collagen fibre orientation and the local mechanical environment. We hypothesize that the low bone matrix volume in the neural spine reduces the need for an extensive osteocyte network, and future research is needed to validate this idea.

7.2 Nederlands

Francis Hamilton ontdekte de zebravis (*Danio rerio*), een van de belangrijkste proefdieren voor het bestuderen van de ontwikkeling van gewervelden. Zebravissen hebben veel voordelen, zoals transparante embryo's, uitwendige bevruchting, snelle ontwikkeling en een hoge vruchtbaarheid, waardoor ze zich hebben gevestigd als een zeer waardevol modelorganisme (Buenzli & Sims, 2015; Foessl et al., 2021; Kague & Karasik, 2022). In zijn studie naar acellulariteit bij Teleostei ontdekte Moss (1961) cellulaire botten in de zebravis, wat inhoudt dat de botten osteocyten in hun extracellulaire matrix bevatten. Osteocyten zijn de meest voorkomende cellen in het skelet van zoogdieren (Bonewald, 2011; Kague & Karasik, 2022). Hun dendritische uitlopers kruipen door de cellulaire matrix in canaliculi. Samen met hun cellichamen, die zich in lacunae bevinden, vormen ze een uitgebreid lacuno-canaliculair netwerk in de botten (Buenzli & Sims, 2015). Lange tijd werd gedacht dat deze cellen in het bot inactief waren. Recente studies tonen echter hun cruciale rol als mechanosensoren en mechanotransducers in zoogdierbotten aan. Hierdoor wordt er recentelijk veel onderzoek gedaan naar hun rol in gezonde botstructuren en hun belang bij botziekten, aangezien dit een groeiend probleem wordt door de vergrijzing van de maatschappij (Bonewald, 2010, 2011; Kague & Karasik, 2022; Tonelli et al., 2020).

Hoewel de zebravis een populair modelorganisme is, weten we nog steeds weinig over de osteocyten in hun botten. Dit komt mede doordat deze cellen pas laat in de skeletontwikkeling verschijnen (Huysseune, 2000; Witten & Huysseune, 2009). Sommige onderzoeken beweerden zelfs dat zebravissen acellulaire botten hebben (Weigele & Franz-Odendaal, 2016), terwijl andere een onderontwikkeld lacuno-canaliculair netwerk vermoeden (Cao et al., 2011), wat essentieel is voor de werking van osteocyten. Aangezien de zebravis steeds vaker wordt gebruikt in botonderzoek en bij het testen van medicijnen, is het van groot belang om de functionaliteit van hun osteocyten en het bijbehorende netwerk op te helderen.

De eerste stap om de kennisklоof te dichten is een nauwkeurige beschrijving van de osteocyten morfologie in het zebravisskelet. Deze studie onderzoekt de verspreiding en morfologische kenmerken van osteocyten in de wervels van de zebravis, met een primaire focus op hun vorm, grootte en de structuur van hun lacuno-canaliculair netwerk. Het onderzoek wil de relatie tussen de morfologie van osteocyten en de rangschikking van de omringende collageenvezels begrijpen. Op basis van bestaande literatuur veronderstelt de studie dat de vorm en dichtheid van osteocyten beïnvloed worden door bottypologie en mechanische belasting, en dat zebravissen een onderontwikkeld dendritisch vertakkingsnetwerk bezitten. Door deze cellen beter te begrijpen, kunnen we zorgen voor een efficiënt gebruik van de zebravis als modelorganisme en de effectiviteit van medicijntesten verbeteren.

Dit onderzoek focust op de osteocyten populatie in de caudale wervels van de zebravis, een skeletelement dat ideaal is vanwege zijn dynamische mechanische omgeving. De wervels bestaan uit een wervellichaam, neurale en hemale bogen/stekels en dorsale, ventrale en laterale trabeculaire platen, waardoor ze distincte mechanische gebieden voor analyse verschaffen.

Voor de karakterisering van de osteocyten maakten we gebruik van histologie met zowel licht- als gepolariseerde lichtmicroscopie. Deze methode is gekozen vanwege de bekende correlatie tussen de oriëntatie van collageenvezels en de lange as van osteocyten, een relatie die het best zichtbaar is onder gepolariseerd licht. We voerden zowel kwantitatieve als kwalitatieve analyses uit op de osteocyten uit elke wervelregio. De kwalitatieve analyse richtte zich op het beschrijven van osteocyten morfologie, oriëntatie en verspreiding in verschillende regio's van de wervel. De kwantitatieve analyse bestond uit het bepalen van de osteocyten dichtheid (cellulariteit) door het aantal osteocyten in elke regio te tellen en te delen door de totale onderzochte oppervlakte. Morfologie werd ook beschreven door de lengte en diameter van de cel te meten met behulp van Fiji. Statistische vergelijkingen van de osteocyten morfologie tussen de verschillende wervelregio's werden uitgevoerd met een ANOVA, gevolgd door post-hoc analyses om significante verschillen te identificeren.

Uit onze metingen bleek dat de osteocyten in de wervels een variabele lengte hadden van 6,114 tot 38,575 µm en diameter van 1,383 tot 9,352 µm. We constateerden significante morfologische verschillen, zowel binnen afzonderlijke wervelregio's als tussen deze regio's onderling. In alle gebieden behalve de neurale stekel identificeerden we twee

belangrijke morfologieën. De eerste bestond uit ronde tot onregelmatig gevormde osteocyten, die hun dendritische uitlopers in alle richtingen uitstraalden zonder een specifieke oriëntatie. Deze kwamen vooral voor in nieuw botweefsel en in overgangszones. De tweede groep waren spoelvormige osteocyten, waarvan de dendritische uitlopers zich in twee loodrechte richtingen uitstrekten. De lange as deze osteocyten volg de richting van de collageenvezels. Een opvallende vondst was de aanwezigheid van een unieke populatie van zeer dunne, langwerpige osteocyten in de neurale doorn. Deze cellen hadden een gemiddelde lengte van 24,757 µm (±5,673 µm) en een gemiddelde diameter van 2,643 µm (±1,096 µm), waardoor ze duidelijk verschilden van osteocyten in andere regio's. Bijzonder was dat deze cellen geen dendritische uitlopers hadden die vanuit het cellichaam uitkwamen en dat de neurale doorn zelf een lage cellulaire dichtheid vertoonde.

De dichtheid van osteocyten verschilde significant, zowel binnen als tussen de wervelregio's. De hoogste dichtheid werd gevonden in de neurale en hemale bogen, gevolgd door de trabeculaire platen. Het centrum, de neurale doorn en de neurale basis daarentegen vertoonden lagere dichtheden. Een interessante bevinding was de hoge dichtheid van zowel de osteocyt-cellichamen als hun dendritische uitlopers in de eindplaten, met name de plekken die loodrecht op de Sharpey-vezels stonden. Deze heterogeniteit in osteocyten dichtheid binnen het wervellichaam wijst op een gelokaliseerde respons op de mechanische omgeving.

De resultaten van de studie bevestigen onze oorspronkelijke hypothese: het type bot beïnvloedt de morfologie en oriëntatie van de osteocyten in de wervels van zebravissen aanzienlijk. Er is een duidelijk verband tussen de vorm van osteocyten en de richting van de collageenvezels in de omringende botmatrix. In georganiseerd (lamellair) bot liggen osteocyten en hun uitlopers sterk in lijn met de collageenvezels, terwijl dit minder duidelijk is in woven bot.

Terwijl het algemene bot type een belangrijke factor is, suggereert de studie dat ook de lokale botarchitectuur en mechanische belasting een cruciale rol spelen. De aanwezigheid van rondere osteocyten in georganiseerd bot, met name in overgangszones waar de oriëntatie van collageenvezels abrupt verandert, wijst bijvoorbeeld op de invloed van de directe mechanische omgeving. Een opvallende gelijkenis werd waargenomen tussen de osteocyten in de neurale doorn en die in de intermusculaire botten (Hall, 2015; Lyall et al., 2024; Nie et al., 2022). Dit is vooral interessant omdat beide gebieden onderhevig zijn aan hoge mechanische eisen, zoals uitgebreide spieraanhechting. Deze observatie suggereert dat specifieke, hoge mechanische krachten de vorm van osteocyten direct kunnen beïnvloeden. De tekst biedt echter ook een alternatieve verklaring: het lage botmatrixvolume dat in deze gebieden wordt gevonden, zou ook een bijdragende factor kunnen zijn.

Dit onderzoek onthult een uitgebreid en zeer georganiseerd osteocytennetwerk in de wervels van de zebravis (*Danio rerio*), wat in tegenspraak is met sommige eerdere studies, maar wel overeenkomt met de bevindingen van andere recente onderzoeken. Daarnaast werd er een duidelijke relatie gevonden tussen plekken met hoge mechanische belasting en een hoge osteocyten dichtheid, wat suggereert dat osteocyten functioneren als mechanosensoren. De ongelijkmatige verdeling van de osteocyten versterkt dit idee: ze hopen zich op in het centrum, vooral bij de Sharpey-vezels die de spieren aan het bot vastmaken (Hall, 2015; Moss, 1961; Witten & Hall, 2003). Deze clustering toont aan dat de verspreiding van osteocyten nauw verbonden is met de lokale mechanische belasting.

De aanzienlijke kennisklоof over osteocyten bij zebravissen vormt een belemmering voor onderzoek naar skeletziekten. Deze studie heeft aangetoond dat de zebravis een uitgebreid, mechanosensitief osteocytennetwerk in de wervels bezit. De dichtheid en verdeling van deze cellen variëren afhankelijk van de mechanische belasting, wat de zebravis tot een veelbelovend model maakt voor het onderzoeken van de rol van matige krachten in het behoud van gezonde botten. Bovendien vertoont de morfologie van de osteocyten in de zebravis, net als bij zoogdieren, een correlatie met de collageenvezels en de lokale mechanische omgeving. Verder onderzoek is nodig om de hypothese te valideren dat het geringe botmatrixvolume in de neurale doorn de behoefte aan een uitgebreid osteocytennetwerk reduceert.

8 Reference list

Atkins, A., Milgram, J., Weiner, S., & Shahar, R. (2015). The response of anosteocytic bone to controlled loading. *Journal of Experimental Biology*, *218*(22), 3559–3569. https://doi.org/10.1242/jeb.124073

Bek, J. W., De Clercq, A., Coucke, P. J., & Willaert, A. (2021). The ZE-Tunnel: An Affordable, Easy-to-Assemble, and User-Friendly Benchtop Zebrafish Swim Tunnel. *Zebrafish*, *18*(1), 29-41. https://doi.org/10.1089/zeb.2020.1948

Bird, N. C., & Mabee, P. M. (2003). Developmental Morphology of the Axial Skeleton of the Zebrafish, Danio rerio (Ostariophysi: Cyprinidae). In *Developmental Dynamics* (Vol. 228, Issue 3, pp. 337–357). https://doi.org/10.1002/dvdy.10387

Bonewald, L. F. (2004). Osteocyte biology: Its implications for osteoporosis. *Journal of Musculoskeletal & Neuronal Interactions*, *4*(1), 101–104.

Bonewald, L. F. (2010). Cell Signaling: Yesterday, Today, and Tomorrow. In *Handbook of Cell Signaling, Second Edition* (Vol. 1, pp. 2647–2662). Elsevier. https://doi.org/10.1016/B978-0-12-374145-5.00001-2

Bonewald, L. F. (2011). The amazing osteocyte. *Journal of Bone and Mineral Research*, *26*(2), 229–238. https://doi.org/10.1002/jbmr.320

Bonewald, L. F., & Johnson, M. L. (2008). Osteocytes, mechanosensing and Wnt signaling. In *Bone* (Vol. 42, Issue 4, pp. 606–615). https://doi.org/10.1016/j.bone.2007.12.224

Bonucci, E. (2009). The osteocyte: the underestimated conductor of the bone orchestra. *Rendiconti Lincei. Scienze Fisiche e Naturali*, *20*, 237–254. https://doi.org/D0I10.1007/sl22l0-009-0051-y

Buenzli, P. R., & Sims, N. A. (2015). Quantifying the osteocyte network in the human skeleton. *Bone*, *75*, 144–150. https://doi.org/10.1016/j.bone.2015.02.016

Burger, E. H., Klein-Nulend, J., & Smit, T. H. (2003). Strain-derived canalicular fluid flow regulates osteoclast activity in a remodelling osteon - A proposal. *Journal of Biomechanics*, *36*(10), 1453–1459. https://doi.org/10.1016/S0021-9290(03)00126-X

Burger, E. H., Klein-Nulend, J., Van Der Plas, A., & Peter, J. N. (1995). Function of Osteocytes in Bone - Their Role in Mechanotransduction. In *Bone and Mineral Research J. Nutr* (Vol. 125). https://academic.oup.com/jn/article-abstract/125/suppl_7/2020S/4730920

Cao, L., Moriishi, T., Miyazaki, T., Iimura, T., Hamagaki, M., Nakane, A., Tamamura, Y., Komori, T., & Yamaguchi, A. (2011). Comparative morphology of the osteocyte lacunocanalicular system in various vertebrates. *Journal of Bone and Mineral Metabolism*, *29*(6), 662–670. https://doi.org/10.1007/s00774-011-0268-6

Creecy, A., Damrath, J. G., & Wallace, J. M. (2021). Control of Bone Matrix Properties by Osteocytes. In *Frontiers in Endocrinology* (Vol. 11). Frontiers Media S.A. https://doi.org/10.3389/fendo.2020.578477

Davesne, D., Meunier, F. J., Schmitt, A. D., Friedman, M., Otero, O., & Benson, R. B. J. (2019). The phylogenetic origin and evolution of acellular bone in teleost fishes: insights into osteocyte function in bone metabolism. *Biological Reviews*, *94*(4), 1338–1363. https://doi.org/10.1111/brv.12505

Davesne, D., Schmitt, A. D., Fernandez, V., Benson, R. B. J., & Sanchez, S. (2020a). Three-dimensional characterization of osteocyte volumes at multiple scales, and its relationship with bone biology and genome evolution in ray-finned fishes. *Journal of Evolutionary Biology*, *33*(6), 808–830. https://doi.org/10.1111/jeb.13612

Davesne, D., Schmitt, A. D., Fernandez, V., Benson, R. B. J., & Sanchez, S. (2020b). Three-dimensional characterization of osteocyte volumes at multiple scales, and its relationship with bone biology and genome evolution in ray-finned fishes. *Journal of Evolutionary Biology*, *33*(6), 808–830. https://doi.org/10.1111/jeb.13612

de Azevedo, A. M., Losada, A. P., Vázquez, S., Witten, P. E., Quiroga, M. I., & Gavaia, P. J. (2025). The Vertebral Column of Flatfish: A Review. In *Reviews in Aquaculture* (Vol. 17, Issue 4). John Wiley and Sons Inc. https://doi.org/10.1111/raq.70056

de Azevedo, T. P., Witten, P. E., Huysseune, A., Bensimon-Brito, A., Winkler, C., To, T. T., & Palmeirim, I. (2012). Interrelationship and modularity of notochord and somites: A comparative view on zebrafish and chicken vertebral body development. In *Journal of Applied Ichthyology* (Vol. 28, Issue 3, pp. 316–319). https://doi.org/10.1111/j.1439-0426.2012.01987.x

Deschamps, M. H., Girondot, M., Labbé, L., & Sire, J. Y. (2009). Changes in vertebral structure during growth of reared rainbow trout, Oncorhynchus mykiss (Walbaum): A new approach using modelling of vertebral bone profiles. *Journal of Fish Diseases*, *32*(3), 233–246. https://doi.org/10.1111/j.1365-2761.2008.00979.x

Fatima, M., Canhao, H., & Eurico, J. (2011). Bone: A Composite Natural Material. In *Advances in Composite Materials - Analysis of Natural and Man-Made Materials*. InTech. https://doi.org/10.5772/17523

Foessl, I., Bassett, J. H. D., Bjørnerem, Å., Busse, B., Calado, Â., Chavassieux, P., Christou, M., Douni, E., Fiedler, I. A. K., Fonseca, J. E., Hassler, E., Högler, W., Kague, E., Karasik, D., Khashayar, P., Langdahl, B. L., Leitch, V. D., Lopes, P., Markozannes, G., … Obermayer-Pietsch, B. (2021). Bone Phenotyping Approaches in Human, Mice and Zebrafish – Expert Overview of the EU Cost Action GEMSTONE ("GEnomics of MusculoSkeletal traits TranslatiOnal NEtwork"). In *Frontiers in Endocrinology* (Vol. 12). Frontiers Media S.A. https://doi.org/10.3389/fendo.2021.720728

Franz-Odendaal, T. A., Hall, B. K., & Witten, P. E. (2006). Buried alive: How osteoblasts become osteocytes. In *Developmental Dynamics* (Vol. 235, Issue 1, pp. 176–190). https://doi.org/10.1002/dvdy.20603

Hall, B. K. . (2015). *Bones and Cartilage: Developmental and Evolutionary Skeletal Biology. 9: Tendon Skeletogenesis and sesamoids* (second edition, pp. 137–149). Elsevier Ltd.

Hamilton, F. (1822). *An account of the fishes found in the river ganges and its branches*.

Haridy, Y., Osenberg, M., Hilger, A., Manke, I., Davesne, D., & Witzmann, F. (2021). Bone metabolism and evolutionary origin of osteocytes: Novel application of FIB-SEM tomography. *Sci. Adv*, *7*, 9113–9144.

Huysseune, A. (2000). Skeletal System. In *Microscopic functional anatomy* (pp. 307–317). Academic Press.

Kague, E., & Karasik, D. (2022). Functional Validation of Osteoporosis Genetic Findings Using Small Fish Models. In *Genes* (Vol. 13, Issue 2). MDPI. https://doi.org/10.3390/genes13020279

Kague, E., Kwon, R. Y., Busse, B., Witten, P. E., & Karasik, D. (2024). Standardization of bone morphometry and mineral density assessments in zebrafish and other small laboratory fishes using X-ray radiography and micro-computed tomography. *Journal of Bone and Mineral Research*, *39*(12), 1695–1710. https://doi.org/10.1093/jbmr/zjae171

Kague, E., Turci, F., Newman, E., Yang, Y., Brown, K. R., Aglan, M. S., Otaify, G. A., Temtamy, S. A., Ruiz-Perez, V. L., Cross, S., Royall, C. P., Witten, P. E., & Hammond, C. L. (2021). 3D assessment of intervertebral disc degeneration in zebrafish identifies changes in bone density that prime disc disease. *Bone Research*, *9*(1). https://doi.org/10.1038/s41413-021-00156-y

Kerschnitzki, M., Wagermaier, W., Roschger, P., Seto, J., Shahar, R., Duda, G. N., Mundlos, S., & Fratzl, P. (2011). The organization of the osteocyte network mirrors the extracellular matrix orientation in bone. *Journal of Structural Biology*, *173*(2), 303–311. https://doi.org/10.1016/j.jsb.2010.11.014

Knothe Tate, M. L., Adamson, J. R., Tami, A. E., & Bauer, T. W. (2004). The osteocyte. In *International Journal of Biochemistry and Cell Biology* (Vol. 36, Issue 1, pp. 1–8). Elsevier Ltd. https://doi.org/10.1016/S1357-2725(03)00241-3

Kwiecinski, G. G., Krook, L., & Wimsatt, W. A. (1987). Annual Skeletal Changes in the Little Brown Bat, Myotis hcifugus lucifugus, With Particular Reference to Pregnancy and Lactation. In *THE AMERICAN JOURNAL OF ANATOMY* (Vol. 178).

Lyall, B. A., Witten, P. E., Carter, C. G., Perrott, M. R., Symonds, J. E., Walker, S. P., Waddington, Z., & Amoroso, G. (2024). The problems with pin bones: Intermuscular bone development and function in salmonids and their implications for aquaculture. In *Reviews in Aquaculture* (Vol. 16, Issue 4, pp. 1981–1995). John Wiley and Sons Inc. https://doi.org/10.1111/raq.12942

Martini, A., Sahd, L., Rücklin, M., Huysseune, A., Hall, B. K., Boglione, C., & Witten, P. E. (2023). Deformity or variation? Phenotypic diversity in the zebrafish vertebral column. *Journal of Anatomy*, *243*(6), 960–981. https://doi.org/10.1111/joa.13926

Moharrer, Y., & Boerckel, J. D. (2021). Tunnels in the rock: Dynamics of osteocyte morphogenesis. In *Bone* (Vol. 153). Elsevier Inc. https://doi.org/10.1016/j.bone.2021.116104

Moss, M. L. (1961). Studies of the acellular bone of teleost fish. 1. Morphological and systematic variations. *Acta Anat.*, *46*, 343–462.

Nie, C. H., Wan, S. M., Chen, Y. L., Huysseune, A., Wu, Y. M., Zhou, J. J., Hilsdorf, A. W. S., Wang, W. M., Witten, P. E., Lin, Q., & Gao, Z. X. (2022). Single-cell transcriptomes and runx2b-/-mutants reveal the genetic signatures of intermuscular bone formation in zebrafish. *National Science Review*, *9*(11). https://doi.org/10.1093/nsr/nwac152

Ofer, L., Dean, M. N., Zaslansky, P., Kult, S., Shwartz, Y., Zaretsky, J., Griess-Fishheimer, S., Monsonego-Ornan, E., Zelzer, E., & Shahar, R. (2019). A novel nonosteocytic regulatory mechanism of bone modeling. *PLoS Biology*, *17*(2). https://doi.org/10.1371/journal.pbio.3000140

Oxlund, H., Barckman, M., Ortoft, G., & Andreassen, T. T. (1995). Reduced concentrations of collagen cross-links are associated with reduced strength of bone. *Bone*, *17*(4), 365–371.

Pei, S. ;, Wang, S. ;, Martinez, J. R. ;, Parajuli, A. ;, & Kirn-Safran, C. B. ; (2021). Osteocytic Pericellular Matrix (PCM): Accelerated Degradation under In Vivo Loading and Unloading Conditions Using a Novel Imaging Approach. *Genes*. https://doi.org/10.3390/genes

Peskin, B., Henke, K., Cumplido, N., Treaster, S., Harris, M. P., Bagnat, M., & Arratia, G. (2020). Notochordal Signals Establish Phylogenetic Identity of the Teleost Spine. *Current Biology*, *30*(14), 2805-2814.e3. https://doi.org/10.1016/j.cub.2020.05.037

Qing, H., Ardeshirpour, L., Divieti Pajevic, P., Dusevich, V., Jähn, K., Kato, S., Wysolmerski, J., & Bonewald, L. F. (2012). Demonstration of osteocytic perilacunar/canalicular remodeling in mice during lactation. *Journal of Bone and Mineral Research*, *27*(5), 1018–1029. https://doi.org/10.1002/jbmr.1567

Sakashita, M., Sato, M., & Kondo, S. (2019). Comparative morphological examination of vertebral bodies of teleost fish using high-resolution micro-CT scans. *Journal of Morphology*, *280*(6), 778–795. https://doi.org/10.1002/jmor.20983

Schindelin, J., Arganda-Carreras, I., Frise, E., Kaynig, V., Longair, M., Pietzsch, T., Preibisch, S., Rueden, C., Saalfeld, S., Schmid, B., Tinevez, J. Y., White, D. J., Hartenstein, V., Eliceiri, K., Tomancak, P., & Cardona, A. (2012). Fiji: An open-source platform for biological-image analysis. In *Nature Methods* (Vol. 9, Issue 7, pp. 676–682). https://doi.org/10.1038/nmeth.2019

Shahar, R., & Dean, M. N. (2013). The enigmas of bone without osteocytes. *BoneKEy Reports*, *2*. https://doi.org/10.1038/bonekey.2013.77

Shiflett, L. A., Tiede-Lewis, L. A. M., Xie, Y., Lu, Y., Ray, E. C., & Dallas, S. L. (2019). Collagen Dynamics During the Process of Osteocyte Embedding and Mineralization. *Frontiers in Cell and Developmental Biology*, *7*. https://doi.org/10.3389/fcell.2019.00178

Suniaga, S., Rolvien, T., Vom Scheidt, A., Fiedler, I. A. K., Bale, H. A., Huysseune, A., Witten, P. E., Amling, M., & Busse, B. (2018). Increased mechanical loading through controlled swimming exercise induces bone formation and mineralization in adult zebrafish. *Scientific Reports*, *8*(1). https://doi.org/10.1038/s41598-018-21776-1

Tauer, J. T., Thiele, T., Julien, C., Ofer, L., Zaslansky, P., Shahar, R., & Willie, B. M. (2024). Swim training induces distinct osseous gene expression patterns in anosteocytic and osteocytic teleost fish. *Bone*, *185*. https://doi.org/10.1016/j.bone.2024.117125

Tonelli, F., Bek, J. W., Besio, R., De Clercq, A., Leoni, L., Salmon, P., Coucke, P. J., Willaert, A., & Forlino, A. (2020). Zebrafish: A Resourceful Vertebrate Model to Investigate Skeletal Disorders. In *Frontiers in Endocrinology* (Vol. 11). Frontiers Media S.A. https://doi.org/10.3389/fendo.2020.00489

Totland, G. K., Fjelldal, P. G., Kryvi, H., Løkka, G., Wargelius, A., Sagstad, A., Hansen, T., & Grotmol, S. (2011). Sustained swimming increases the mineral content and osteocyte density of salmon vertebral bone. *Journal of Anatomy*, *219*(4), 490–501. https://doi.org/10.1111/j.1469-7580.2011.01399.x

Viguet-Carrin, S., Garnero, P., & Delmas, P. D. (2006). The role of collagen in bone strength. In *Osteoporosis International* (Vol. 17, Issue 3, pp. 319–336). https://doi.org/10.1007/s00198-005-2035-9

Veno P, Nicolella DP, Sivakumar P, Kalajzic I, Rowe D, Harris SE, Bonewald L, Dallas SL. Live imaging ofosteocytes within their lacunae reveals cell body and dendrite motions. J Bone Miner Res 2006;21 (Suppl 1): S38.

Wang, L. (2018). Solute Transport in the Bone Lacunar-Canalicular System (LCS). In *Current Osteoporosis Reports* (Vol. 16, Issue 1, pp. 32–41). Current Medicine Group LLC 1. https://doi.org/10.1007/s11914-018-0414-3

Weigele, J., & Franz-Odendaal, T. A. (2016). Functional bone histology of zebrafish reveals two types of endochondral ossification, different types of osteoblast clusters and a new bone type. *Journal of Anatomy*, *229*(1), 92–103. https://doi.org/10.1111/joa.12480

Witten, P. E., & Hall, B. K. (2003). Seasonal changes in the lower jaw skeleton in male Atlantic salmon (Salmo salar L.): Remodelling and regression of the kype after spawning. *Journal of Anatomy*, *203*(5), 435–450. https://doi.org/10.1046/j.1469-7580.2003.00239.x

Witten, P. E., & Hall, B. K. (2015). Teleost Skeletal Plasticity: Modulation, Adaptation, and Remodelling. *Copeia*, *103*(4), 727–739. https://doi.org/10.1643/CG-14-140

Witten, P. E., Harris, M. P., Huysseune, A., & Winkler, C. (2017). Small teleost fish provide new insights into human skeletal diseases. *Methods in Cell Biology*, *138*, 321–346. https://doi.org/10.1016/bs.mcb.2016.09.001

Witten, P. E., & Huysseune, A. (2009). A comparative view on mechanisms and functions of skeletal remodelling in teleost fish, with special emphasis on osteoclasts and their function. *Biological Reviews*, *84*(2), 315–346. https://doi.org/10.1111/j.1469-185X.2009.00077.x

Witten PE, Hansen A, Hall BK. Features of mono- and multinucleated bone resorbing cells of the zebrafish Danio rerio and their contribution to skeletal development, remodeling, and growth. J Morphol. 2001 Dec;250(3):197-207. doi: 10.1002/jmor.1065. PMID: 11746460.

For this dissertation, I used generative AI tools for writing assistance. Google Gemini and Grammarly were both employed to perform grammatical corrections and to rephrase sentences. Additionally, Google Gemini was used to assist in the construction of image legends. All content generated by these tools was critically reviewed and adapted to fit the academic context of this work.

9 Appendix

9.1 Length

Table 4. result of the Games Howell Post Hoc analyses on osteocyte length in different regions of the vertebrae. green indicates significant p-values on the 0.05 significance scale. (C: Centrum (endplates + vertebral body), C-NB: transition Centrum and Neural Base, DT: dorsal trabeculation, H: heamal arch, LT: Lateral Trabeculation, N: Neural Arch, NB: Neural Base, NS: Neural Spine, VT: Ventral trabeculation)

	C	C-NB	DT	H	LT	N	NB	NS
C-NB	-	-	-	-	-	-	-	-
DT	0.9944	1,0000	-	-	-	-	-	-
H	1,0000	0.9653	0,9959	-	-	-	-	-
LT	0.5998	0.9229	0.8663	0,6211	-	-	-	-
N	0.8010	0.9962	0.9887	0.8306	0,9994	-	-	-
NB	-	-	-	-	-	-	-	-
NS	0.0025	0.0698	0.0067	0.0023	0.6383	0.1213	-	-
VT	0.0172	0.781	0.5206	0.0996	1,000	1,000	-	0.0753

9.2 Diameter

Table 5: Post-Hoc Analysis of Cell Diameter in Different Bone Regions. with Bonferroni correction was performed to adjust for multiple comparisons. The table includes the mean difference between groups, the 95% confidence interval for the difference, and the adjusted *p*-value. An adjusted *p*-value of less than 0.05 indicates a statistically significant difference between the two groups. Significant differences are marked with an asterisk (*) and indicated in green.

regio	diff	lwr,ci	upr,ci	pval	sign
C-NB-C	-1,2483	-5,9288	3,4323	1,0000	
DT-C	-0,1173	-0,9011	0,6665	1,0000	
H-C	0,0195	-0,8729	0,9118	1,0000	
LT-C	-0,0563	-1,0502	0,9376	1,0000	
N-C	-0,2057	-1,0903	0,6788	1,0000	
NB-C	-0,1488	-1,7762	1,4785	1,0000	
NS-C	-1,5977	-2,8606	-0,3348	0,0020	**
VT-C	0,4810	-0,2701	1,2321	1,0000	
DT-C-NB	1,1310	-3,5637	5,8257	1,0000	
H-C-NB	1,2678	-3,4463	5,9818	1,0000	
LT-C-NB	1,1920	-3,5423	5,9263	1,0000	
N-C-NB	1,0426	-3,6700	5,7552	1,0000	
NB-C-NB	1,0994	-3,8071	6,0060	1,0000	
NS-C-NB	-0,3494	-5,1474	4,4486	1,0000	
VT-C-NB	1,7293	-2,9601	6,4187	1,0000	
H-DT	0,1368	-0,8271	1,1007	1,0000	
LT-DT	0,0610	-0,9976	1,1196	1,0000	
N-DT	-0,0884	-1,0451	0,8683	1,0000	
NB-DT	-0,0315	-1,6992	1,6361	1,0000	
NS-DT	-1,4804	-2,7949	-0,1660	0,0117	*

VT-DT	0,5983	-0,2365	1,4332	0,7730	
LT-H	-0,0758	-1,2171	1,0656	1,0000	
N-H	-0,2252	-1,2727	0,8223	1,0000	
NB-H	-0,1683	-1,8897	1,5530	1,0000	
NS-H	-1,6172	-2,9991	-0,2353	0,0069	**
VT-H	0,4615	-0,4760	1,3990	1,0000	
N-LT	-0,1494	-1,2847	0,9858	1,0000	
NB-LT	-0,0926	-1,8687	1,6835	1,0000	
NS-LT	-1,5414	-2,9910	-0,0919	0,0246	*
VT-LT	0,5373	-0,4974	1,5720	1,0000	
NB-N	0,0569	-1,6604	1,7742	1,0000	
NS-N	-1,3920	-2,7689	-0,0151	0,0443	*
VT-N	0,6867	-0,2434	1,6168	0,6429	
NS-NB	-1,4489	-3,3884	0,4906	0,5964	
VT-NB	0,6299	-1,0227	2,2824	1,0000	
VT-NS	2,0787	0,7835	3,3739	0,0000	***

9.3 Volume

Table 6. Post-Hoc pairwise comparisons of cell volume. The table includes the mean rank differences, the Dunn's test statistic (Z), the unadjusted *p*-value, and the adjusted *p*-value (P.adj) using the Holm method. An adjusted *p*-value less than 0.05 indicates a statistically significant difference between the two compared groups. Significant differences are marked with an asterisk (*) and indicated in green.

Comparison of x by group									
(Holm)									
		C	**C_NB**	**DT**	**H**	**LT**	**N**	**NB**	**NS**
z value	**C-NB**	0,607575							
p-adjusted		1,000000							
z value	**DT**	0,399039	-0,506586						
p-adjusted		1,000000	1,000000						
z value	**H**	2,158265	0.026699	1,677216					
p-adjusted		0,479100	0,489300	1,000000					
z value	**LT**	0,533206	-0,408180	0,236853	-1,116178				
p-adjusted		1,000000	1,000000	1,000000	1,000000				
z value	**N**	1,482348	-0,230626	0,980432	-0,792941	0,508245			
p-adjusted		1,000000	1,000000	1,000000	1,000000	1,000000			
z value	**NB**	-0.151873	-0.591017	-0.282922	-0.998203	-0.381801	-0.662305		
p-adjusted		1,000000	1,000000	1,000000	1,000000	1,000000	1,000000		
z value	**NS**	1,499369	-0.086762	1,142796	-0.290442	0.753789	0.381718	0,817002	
p-adjusted		1,000000	0,930900	1,000000	1,000000	1,000000	1,000000	1,000000	
z value	**VT**	-2,477968	-1,157674	-2,526969	-3,878341	-2,075043	-3,477975	-0,619469	-3,012127
p-adjusted		0,211400	1,000000	0,189800	0,001900	0,569700	0,008800	1,000000	0,044100

9.4 Ratio

Table 7. Post-Hoc pairwise comparisons of length:diameter ratio. The table shows the comparison groups, their respective sample sizes (n1 and n2), the Dunn's test statistic, the unadjusted *p*-value, and the Holm-adjusted *p*-value (p.adj). The significance of the adjusted *p*-value is indicated by symbols in the final column: ns (not significant), * (padj<0.05), ** (padj<0.01), and *** (padj<0.001) and indicated in green.

group1	group2	n1	n2	statistic	p	p.adj	p.adj.signif
C	C-NB	46	1	1.205.366.709	2,28E-01	1,00E+00	ns
C	DT	46	26	1.707.651.810	8,77E-02	1,00E+00	ns
C	H	46	15	1.705.040.149	8,82E-02	1,00E+00	ns
C	LT	46	10	2.899.261.145	3,74E-03	1,16E-01	ns
C	N	46	23	2.387.249.950	1,70E-02	5,09E-01	ns
C	NB	46	2	1.672.479.782	9,44E-02	1,00E+00	ns
C	NS	46	10	5.252.430.347	1,50E-07	5,40E-06	****
C	VT	46	34	1.441.691.132	1,49E-01	1,00E+00	ns
C-NB	DT	1	26	-0.784468036	4,33E-01	1,00E+00	ns
C-NB	H	1	15	-0.688845503	4,91E-01	1,00E+00	ns
C-NB	LT	1	10	-0.197188419	8,44E-01	1,00E+00	ns
C-NB	N	1	23	-0.595932233	5,51E-01	1,00E+00	ns
C-NB	NB	1	2	-0.008443104	9,93E-01	1,00E+00	ns
C-NB	NS	1	10	0.585649603	5,58E-01	1,00E+00	ns
C-NB	VT	1	34	-0.879497035	3,79E-01	1,00E+00	ns
DT	H	26	15	0.271331303	7,86E-01	1,00E+00	ns
DT	LT	26	10	1.592.561.069	1,11E-01	1,00E+00	ns
DT	N	26	23	0.666065757	5,05E-01	1,00E+00	ns
DT	NB	26	2	1.075.322.485	2,82E-01	1,00E+00	ns
DT	NS	26	10	3.799.059.774	1,45E-04	4,94E-03	**
DT	VT	26	34	-0.356685314	7,21E-01	1,00E+00	ns
H	LT	15	10	1.236.070.376	2,16E-01	1,00E+00	ns
H	N	15	23	0.309409585	7,57E-01	1,00E+00	ns
H	NB	15	2	0.931351485	3,52E-01	1,00E+00	ns
H	NS	15	10	3.247.217.668	1,17E-03	3,85E-02	*
H	VT	15	34	-0.583615532	5,59E-01	1,00E+00	ns
LT	N	10	23	-1.061.119.711	2,89E-01	1,00E+00	ns
LT	NB	10	2	0.253644662	8,00E-01	1,00E+00	ns
LT	NS	10	10	1.835.917.897	6,64E-02	1,00E+00	ns
LT	VT	10	34	-1.905.618.085	5,67E-02	1,00E+00	ns
N	NB	23	2	0.811721187	4,17E-01	1,00E+00	ns
N	NS	23	10	3.228.700.041	1,24E-03	3,98E-02	*
N	VT	23	34	-1.050.396.457	2,94E-01	1,00E+00	ns
NB	NS	2	10	0.806323030	4,20E-01	1,00E+00	ns
NB	VT	2	34	-1.212.188.160	2,25E-01	1,00E+00	ns
NS	VT	10	34	-4.187.963.508	2,81E-05	9,85E-04	***